USGS
science for a changing world

Prepared in cooperation with the Bernalillo County Public Works Division

Landscape and Climatic Influences on Actual Evapotranspiration and Available Water Using the Operational Simplified Surface Energy Balance (SSEBop) Model in Eastern Bernalillo County, New Mexico, 2015

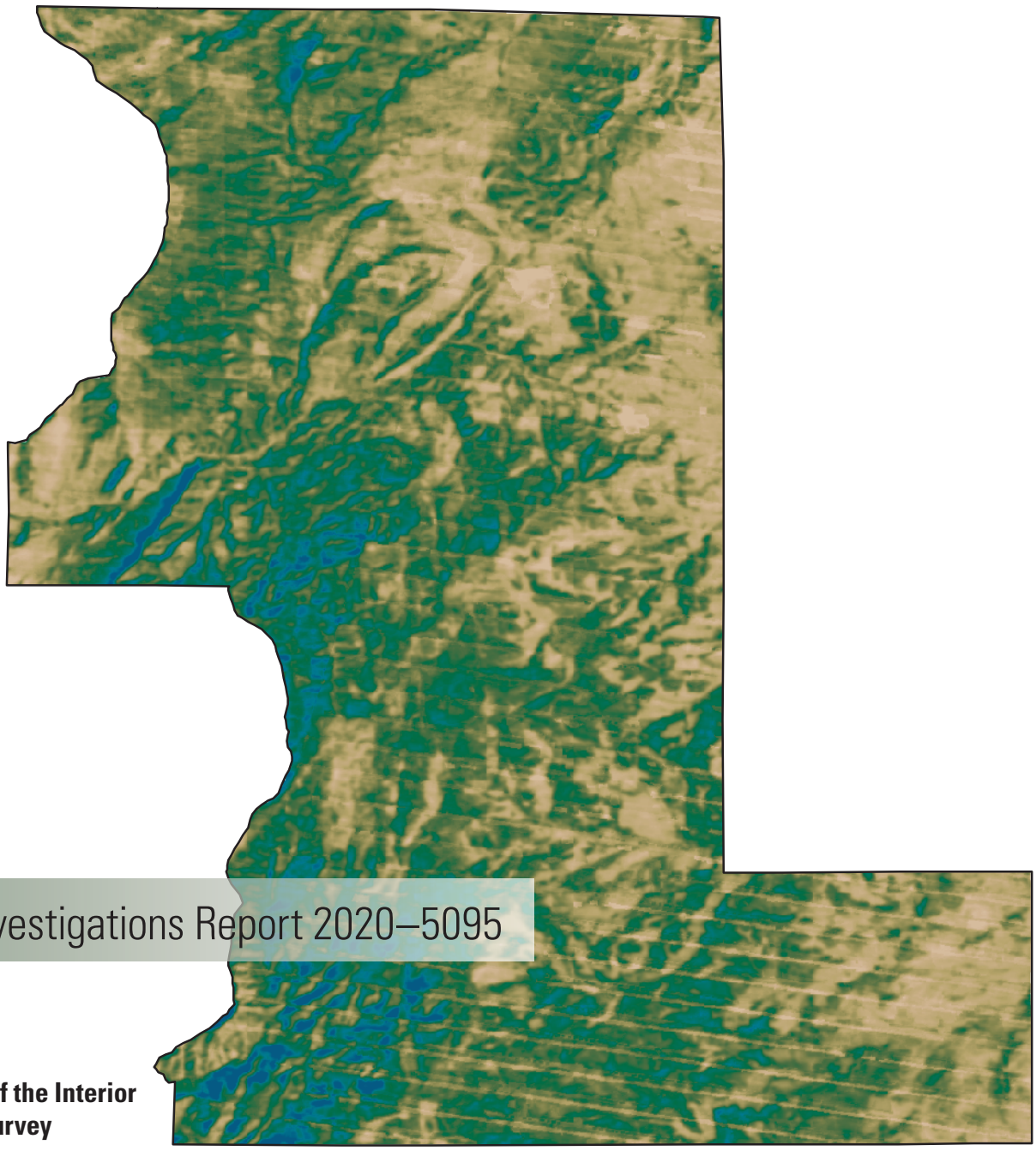

Scientific Investigations Report 2020–5095

U.S. Department of the Interior
U.S. Geological Survey

Cover. Map showing annual actual evapotranspiration (*ETa*) in the East Mountain area of Bernalillo County, New Mexico, 2015. Further details provided on figure 7*A* of this report.

Landscape and Climatic Influences on Actual Evapotranspiration and Available Water Using the Operational Simplified Surface Energy Balance (SSEBop) Model in Eastern Bernalillo County, New Mexico, 2015

By Kyle R. Douglas-Mankin, Ryan J. McCutcheon, Aurelia C. Mitchell, and Gabriel B. Senay

Prepared in cooperation with the Bernalillo County Public Works Division

Scientific Investigations Report 2020–5095

U.S. Department of the Interior
U.S. Geological Survey

U.S. Department of the Interior
DAVID BERNHARDT, Secretary

U.S. Geological Survey
James F. Reilly II, Director

U.S. Geological Survey, Reston, Virginia: 2020

For more information on the USGS—the Federal source for science about the Earth, its natural and living resources, natural hazards, and the environment—visit https://www.usgs.gov or call 1–888–ASK–USGS.

For an overview of USGS information products, including maps, imagery, and publications, visit https://store.usgs.gov.

Suggested citation:
Douglas-Mankin, K.R., McCutcheon, R.J., Mitchell, A.C., and Senay, G.B., 2020, Landscape and climatic influences on actual evapotranspiration and available water using the Operational Simplified Surface Energy Balance (SSEBop) Model in eastern Bernalillo County, New Mexico, 2015: U.S. Geological Survey Scientific Investigations Report 2020–5095, 40 p., https://doi.org/10.3133/sir20201095.

ISSN 2328-0328 (online)

Acknowledgments

The authors gratefully acknowledge Bernalillo County Public Works Natural Resource Services for their cooperation with this investigation. Thanks are due to Dan McGregor, Philip Rust, and Sara Chudnoff of Bernalillo County Public Works Natural Resource Services for their support of this project and for their contributions of time, resources, and technical guidance.

Contents

Figures

Tables

Conversion Factors

International System of Units to U.S. customary units

Multiply	By	To obtain
	Length	
micrometer (μm)	3.937×10^{-5}	inch (in.)
centimeter (cm)	0.3937	inch (in.)
millimeter (mm)	0.03937	inch (in.)
meter (m)	3.281	foot (ft)
kilometer (km)	0.6214	mile (mi)
	Area	
square kilometer (km^2)	247.1	acre
square kilometer (km^2)	0.3861	square mile (mi^2)
	Mass	
kilogram (kg)	2.205	pound avoirdupois (lb)
	Velocity	
meter per second (m/s)	3.281	foot per second (ft/s)
	Precipitation	
millimeter per year (mm/yr)	0.03937	inch per year (in/yr)
	Surface resistance	
second per meter (s/m)	3.282	second per foot (s/ft)
	Energy	
joule (J)	2.78×10^{-7}	kilowatthour (kWh)
megajoule (MJ)	0.278	kilowatthour (kWh)

Temperature in degrees Celsius (°C) may be converted to degrees Fahrenheit (°F) as °F = (1.8 × °C) + 32.

Temperature in Kelvin (K) may be converted to degrees Celsius (°C) as °C = K – 273.15.

Datum

Vertical coordinate information is referenced to the North American Vertical Datum of 1988 (NAVD 88).

Horizontal coordinate information is referenced to the North American Datum of 1983 (NAD 83).

Elevation, as used in this report, refers to distance above the vertical datum.

Abbreviations

AIC	Akaike information criterion
ANOVA	analysis of variance
b	regression intercept
denom df	denominator degrees of freedom
df	degrees of freedom
EROS	Earth Resources Observation and Science
ET	evapotranspiration
ETa	actual evapotranspiration
ETM+	Enhanced Thematic Mapper Plus
ETo	reference evapotranspiration
F	F-statistic
GDAS	Global Data Assimilation System
GIS	geographic information system
Kc	crop coefficient
LAI	leaf area index
m	regression slope
METRIC	Mapping EvapoTranspiration at high Resolution and with Internalized Calibration
MODIS	Moderate Resolution Imaging Spectroradiometer
NDVI	Normalized Difference Vegetation Index
NLCD	National Land Cover Database
NRCS	Natural Resources Conservation Service
p	probability of obtaining a result more extreme than the observed result
P	precipitation
P	precipitation, PRISM parameter
PRISM	Parameter-Elevation Regressions on Independent Slopes Model
PROBA-V	Project for On-Board Autonomy-Vegetation
Q1	first quartile
Q3	third quartile
r	Pearson's r coefficient
R^2	coefficient of determination
SEBAL	Surface Energy Balance Algorithm for Land
SEBS	Surface Energy Balance System
sin	sine
SPOT–4	Satellite Pour l'Observation de la Terre [satellite]
SRTM	Shuttle Radar Topography Mission
SSEBop	Simplified Surface Energy Balance Operationalized [model]
SSURGO	Soil Survey Geographic
Tdp	dewpoint temperature

TIR	thermal infrared
USGS	U.S. Geological Survey
VNIR	visible and near infrared
WSS	Web Soil Survey

Landscape and Climatic Influences on Actual Evapotranspiration and Available Water Using the Operational Simplified Surface Energy Balance (SSEBop) Model in Eastern Bernalillo County, New Mexico, 2015

By Kyle R. Douglas-Mankin, Ryan J. McCutcheon, Aurelia C. Mitchell, and Gabriel B. Senay

Abstract

The U.S. Geological Survey, in cooperation with the Bernalillo County Public Works Division, conducted a 1-year study in 2015 to assess the spatial and temporal distribution of evapotranspiration (ET) and available water within the East Mountain area in Bernalillo County, New Mexico. ET and available water vary spatiotemporally because of complex interactions among environmental factors, including vegetation characteristics, soil characteristics, topography, and climate.

Precipitation data from the Parameter-Elevation Regressions on Independent Slopes Model (PRISM) (*P*) were used in conjunction with actual ET (*ETa*) data from the Operational Simplified Surface Energy Balance (SSEBop) model to estimate available water (*P* – *ETa*) at 100-meter (m) resolution in the study area. Maps, descriptive statistics, boxplots, regression analyses (continuous data), and multiple comparison tests (categorical data) were used to characterize *P*, *ETa*, and available water and their relations to topographic, soil, and vegetation datasets in the East Mountain area. Five categories of the natural land-cover type (evergreen forest, shrub, herbaceous, deciduous forest, and mixed forest) and four categories of developed land-cover type specific to residential intensity (developed open, developed low, developed medium, and developed high) were analyzed individually and in interaction with multiple elevation, tree canopy, and soil texture classes.

Annual mean *P* in 2015 in the East Mountain area was 608 millimeters (mm), and annual mean *ETa* was 543 mm (89 percent of annual *P* in 2015), indicating that in 2015, a spatial mean of about 65 mm of water was available for runoff, soil moisture replenishment, or groundwater recharge. Monthly *ETa* was greatest in July and smallest in January. The intervening months did not show smooth temporal or consistent spatial changes from month to month. Months with lower *ETa* (January to March, October to December) also tended to have greater available water, indicating that soil moisture (water supply) and potential ET (water demand) may have been out of phase.

Regression analyses showed that monthly *ETa* data had the highest correlation with annual *ETa* among the atmospheric, topographic, soil, or vegetation datasets, particularly during the early and late growing season (March, April, May, and September). In contrast, monthly *P* was highly variable and not as highly correlated with annual *ETa*. Among landscape variables, correlations with annual *ETa* were highest for tree canopy cover (coefficient of determination [R^2] = 0.46). Correlations between *ETa* and other landscape variables were lower (R^2 = 0.06–0.19): available soil water in the top 100 centimeters, soil bulk density of layer 1, slope, sand content of soil layer 1, soil depth, available soil water in the top 25 centimeters, leaf area index, aspect eastness, and elevation. Evergreen forest areas had the highest annual median *ETa*, followed by mixed forest, open residential areas, and deciduous forest. Available water typically was higher in landcover types with lower *ETa*: herbaceous cover, followed by deciduous forest, high-intensity developed areas, and shrub. Deciduous forest had the second highest median available water, despite having the fourth highest *ETa*, because deciduous forest had greater *P* than most other areas. Annual median *ETa* typically was greatest in the second highest elevation band (2,401–2,800 m above the North American Vertical Datum of 1988 [NAVD 88]), and lower in the highest elevation band (2,801–3,254 m above NAVD 88), despite having greater *P*, likely because of decreased tree canopy cover or a shift from evergreen to deciduous trees at the highest elevations.

Annual median *ETa* increased with tree canopy cover, regardless of landcover type. *ETa* correlation was higher with tree canopy than with leaf area index or normalized difference vegetation index. This result indicates that it is important to include the thermal band (from satellite multispectral data) in vegetation indices used to describe *ETa*, perhaps to account for the influence of energy limitation or water limitation on ET. Of all natural landcover types, finer soils had the most available water, whereas coarser soils had the least available water. Relations of soil type with *P* – *ETa* were different than with *ETa*, indicating ET and available water have a complex response to differences in soil type. Further

modeling would be useful in determining soils' infiltration, storage, conductivity, and plant-water availability relations to individual storms for each position in the landscape, as well as the corresponding effects of these processes on ET and available water.

The best multivariate linear model for annual *ETa* had an R^2 value of 0.62. Monthly *ETa* models had R^2 values between 0.16 and 0.65. Models usually, but not always, performed best during the growing season. These results indicate that even the best multivariate linear models cannot explain a notable amount of the variability in ET. The monthly *ETa* models with the highest correlations (August and September) followed a July having almost twice the mean precipitation for July (1981–2010), which indicates that a soil-moisture variable is needed to more accurately model monthly *ETa*. Further study is needed to better characterize this system, the variables that affect ET and available water, and the partitioning of available water into runoff, soil moisture storage, and groundwater recharge.

Introduction

The East Mountain area of New Mexico is relatively undeveloped and lies near the city of Albuquerque (population 545,852), the largest metropolitan area in the State (fig. 1; U.S. Census Bureau, 2010). Because of its proximity to Albuquerque, the East Mountain area has the potential for substantial population growth in the near future. This growth would require the development of groundwater resources, which has raised concerns about local groundwater sustainability. Directly related to sustainability is the balance of precipitation (P) and evapotranspiration (ET), referred to as "available water," which strongly influences soil water storage, streamflow, groundwater recharge, and ecosystem function (Amatya and others, 2016).

The U.S. Geological Survey (USGS), in cooperation with the Bernalillo County Public Works Division, conducted a 1-year study in 2015 to assess the spatial and temporal distribution of ET and available water within eastern Bernalillo County, New Mexico. Technical data and interpretation from this study could be used to inform management and future planning of eastern Bernalillo County water resources.

Purpose and Scope

The purpose of this report is to describe the landscape and climatic influences on actual evapotranspiration and available water along the eastern slopes of the Sandia and Manzanita Mountains within the East Mountain area in Bernalillo County, N. Mex. Gridded P data and satellite remote-sensing-based ET data for 2015 were analyzed with a geospatial model to assess both spatial variability and intra-annual variability of ET and available water.

At the time of this report, high-resolution ET data were only available for a single year (2015). As such, the scope and applicability of these analyses and results were constrained by climatic conditions for that year, and extrapolations to other years or climatological conditions are not recommended. Care was taken in this report to note climatological conditions that were present for the time period of this study, how these conditions relate to historical conditions, and how these conditions might have influenced the data, analyses, and results of this study.

Description of Study Area

The East Mountain area consists of approximately 673 square kilometers (260 square miles) in Bernalillo County, east of the crests of the Sandia and Manzanita Mountains (fig. 1). The East Mountain area includes the communities of Carnuel (population 1,232), Cedar Crest (population 958), Tijeras (population 541), Sandia Park (population 237), and Chilili (population 137) (U.S. Census Bureau, 2010). Elevation in the East Mountain area ranges from about 1,750 meters (m) (5,741 feet [ft]) above the North American Vertical Datum of 1988 (NAVD 88) in Tijeras Canyon to 3,257 m (10,686 ft) above NAVD 88 at the crest of the Sandia Mountains (fig. 2). This variation in elevation contributes to variations in temperature, P, and ET in the study area.

Concerning groundwater sustainability, a recent study of groundwater recharge in the East Mountain area found that "the mechanisms for recharge and groundwater movement in the East Mountain area are complex and that factors such as climatic variability, the extent and interconnection of structural features such as faults and fractures, and potential solution enhancement of the aquifers all play important roles in the rates and timing of recharge" (Rice and Crilley, 2014, p. 1). Isotopic analyses indicated the leading source of groundwater recharge was winter P (primarily snow) at higher elevation areas, with a lesser contribution of monsoonal rainfall (Rice and Crilley, 2014).

Annual climate normal data (1981–2010) for the Sandia Park, N. Mex. station (National Oceanic Atmospheric Administration station 298015; fig. 1; Arguez and others, 2012) of the National Oceanic Atmospheric Administration, National Weather Service Cooperative Network are 506.5 millimeters per year (mm/yr) (19.94 inches per year [in/yr]) precipitation, 1,510 mm/yr (59.5 in/yr) snowfall, and 10.6 °C mean temperature. Monthly climate normal data indicate that 55 percent of annual precipitation falls from June to October, and 76 percent of annual precipitation as snow falls from December to March. Mean monthly temperatures (1981–2010) range from 0.2 °C in December to 21.4 °C in July.

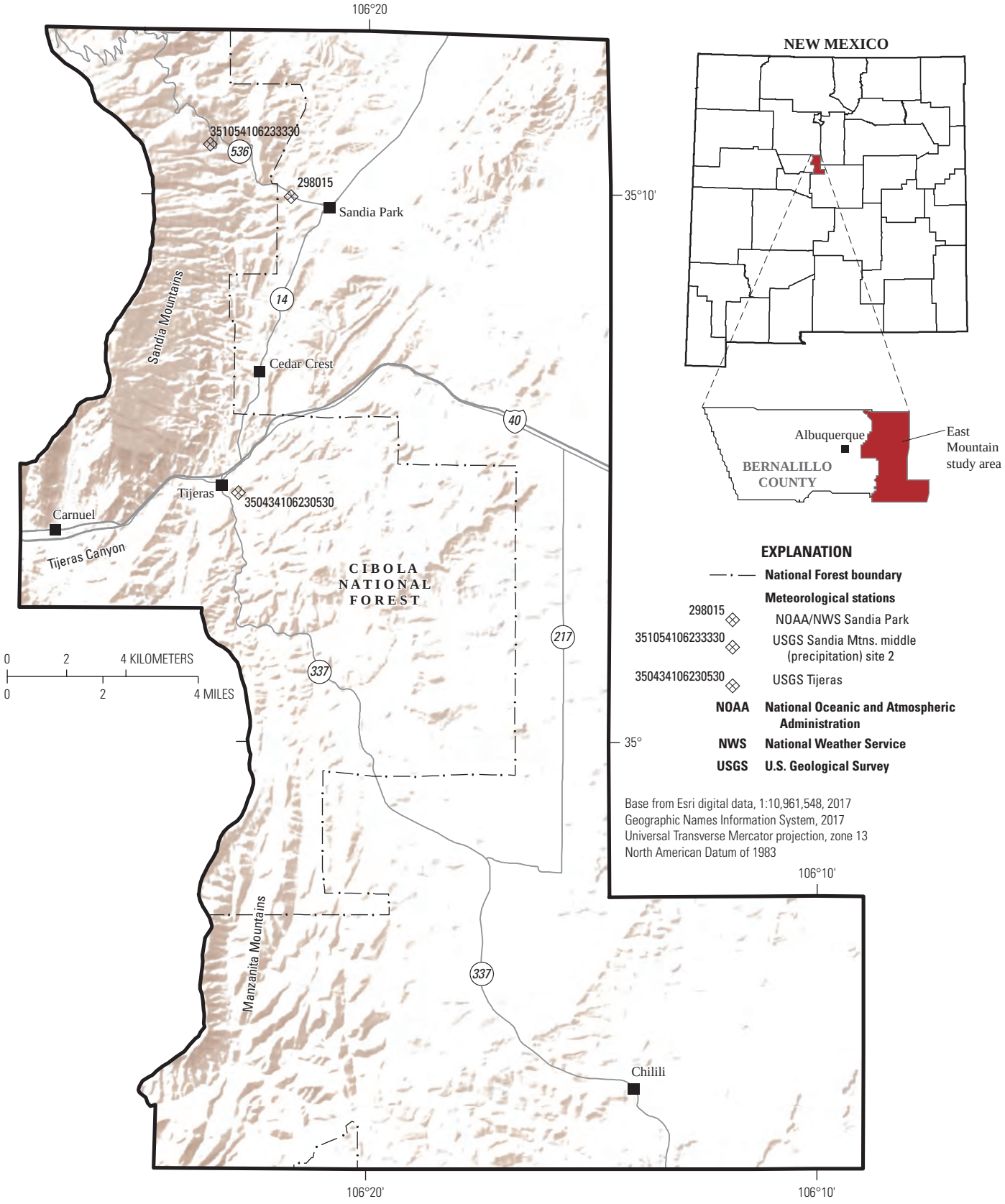

Figure 1. East Mountain area of Bernalillo County, New Mexico.

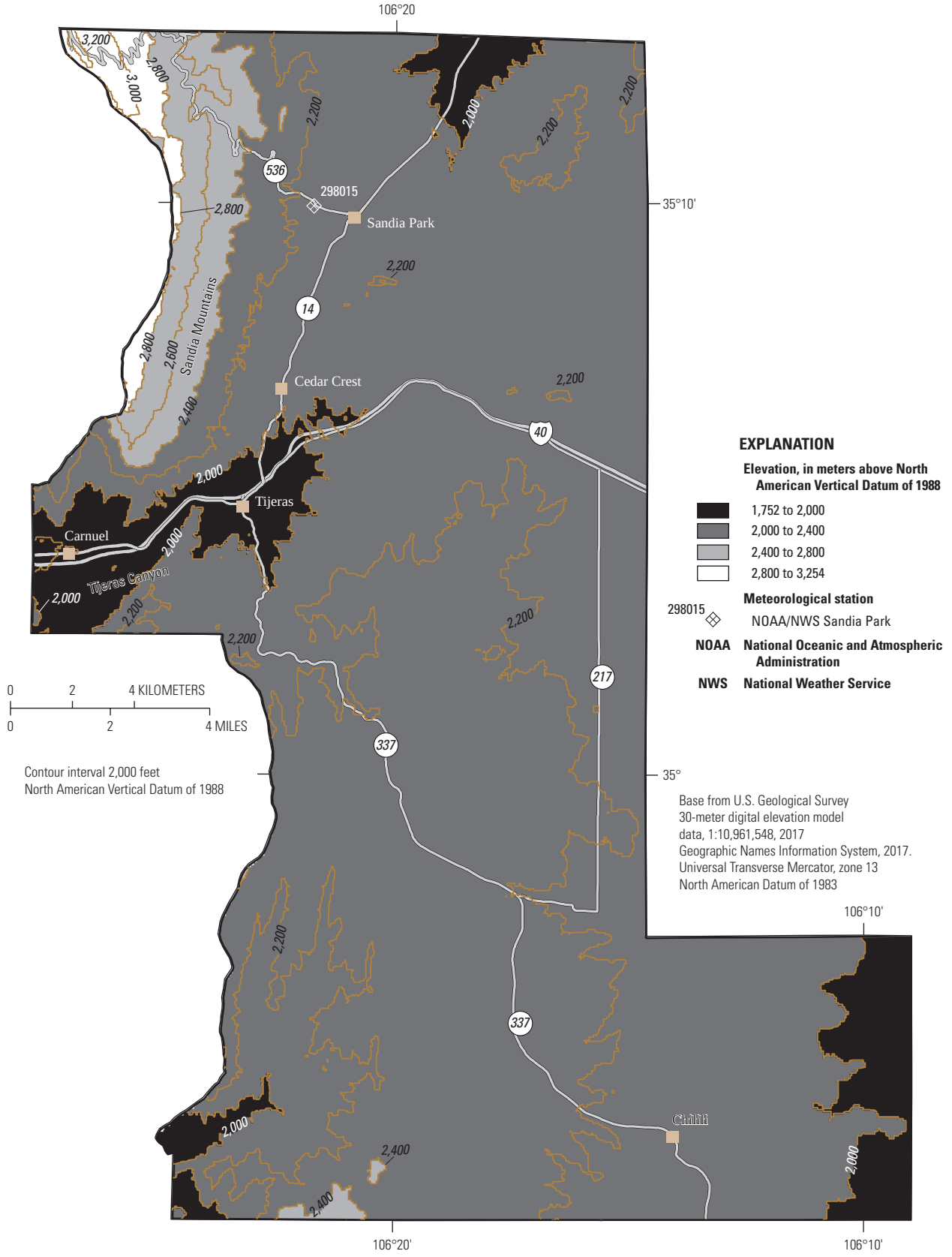

Figure 2. Topography in the East Mountain area of Bernalillo County, New Mexico.

The Köppen-Geiger climate classification uses three letters to characterize world climates based on vegetation group (first letter), precipitation (second letter), and air temperature (third letter) (Kottek and others, 2006). The East Mountain area is classified as a Cfb climate (using 1986–2010 data), which is a warm temperate, fully humid climate with warm summers (Kottek and others, 2006; Rubel and others, 2017). The Cfb classification exists in many of the mountainous regions of New Mexico that fall outside the classification of a snow climate (D, mean temperature of the coldest month is less than (<) −3 °C). This classification is also in contrast to the lower-elevation, arid, steppe climate (BSk, mean annual temperature <18 °C) characteristic of the area immediately west of the Sandia-Manzanita Mountain ridge, including Albuquerque.

Soils in the East Mountain area are predominately Silver and Witt soils (Soil Survey Staff, Natural Resources Conservation Service [NRCS], 2017), which are well drained and classified as hydrologic soil group C, indicating moderately high runoff potential. The soils typically are classified in the Ustollic Haplargid subgroup (fig. 3) and tend to have loamy skeletal or fine particle size. The depth of the first layer is about 130 centimeters (cm), and depth of the top of the restrictive layer can be as great as 1,520 cm. A substantial portion of the remaining soil is Laporte Rock Outcrop and part of the Escabosa complex. A large portion of the remaining soil is in the Ustollic Calciorthid subgroup (fig. 3). These soils also tend to be well drained, are classified as hydrologic group D (indicating high runoff potential), and are loamy in structure. The depth of the first layer of these soils is as great as about 200 cm, and the depth of the top of the restrictive layer is about 480 cm.

Vegetation is primarily evergreen forest (fig. 4) dominated by 40- to 50-percent tree cover (fig. 5) in the spring and summer seasons. Evergreen forest accounts for about 70 percent of the study area, with shrub cover accounting for 12 percent, herbaceous vegetation accounting for 11 percent, and other minor land cover accounting for the last 7 percent (Homer and others, 2015).

Background

ET, the movement of water from land to air by the combined processes of evaporation from free-water surfaces and transpiration through plants, is a fundamental element of hydrologic systems from local to global scales. The balance of P and ET, referred to as “available water,” strongly influences soil water storage, streamflow, groundwater recharge, and ecosystem function (Amatya and others, 2016). ET and available water vary across the landscape and time, owing to the influences of a great variety of factors, including

- land-cover characteristics—vegetative type, age, density, and canopy characteristics, both for individual plants and for local plant communities;
- soil characteristics—including texture, bulk density, surface roughness, and surface residue condition;
- soil-water characteristics—soil-water content, distribution with depth, and capillary movement characteristics;
- topography—at a variety of scales, such as the influence of aspect and slope on exposed surface area, exposure to sun and wind, and interaction with the atmospheric boundary layer;
- exposed surface-water characteristics—ponded-water surface area, temperature, depth, turbidity, and chemistry; and
- climatological factors—including net solar (shortwave) and longwave radiation, boundary layer temperature and vapor pressure, and wind speed and direction (Shuttleworth, 1993; Ward and others, 2004).

ET Measurement Methods

Several methods have been used to measure or provide surrogates for measurement of ET or potential ET (Ward and others, 2004), including measurement of water loss from a pan, quantification of vapor fluxes from a surface (for example, Bowen-ratio energy-budget method, eddy-covariance method), and various models derived from the diffusive flux equation, including the Penman-Monteith (Penman, 1948; Monteith, 1965), Hargreaves-Samani (Hargreaves and Samani, 1985), and others. There is no single “best” method for estimating ET in all situations; each method has its own simplifications, assumptions, and limitations. For example, the Penman-Monteith equation used in this study is derived from the diffusive flux equation in a manner that allows ET to be calculated from readily available meteorological data. Two key assumptions are that the evaporating surface is wet and thus surface temperature equals wet-bulb temperature of the surrounding air and that aerodynamic resistance from the leaf surface through the near-surface atmospheric boundary layer is similar for sensible heat transfer and vapor transfer. An additional assumption is that meteorological conditions measured by a well-maintained weather station at 2 meters (m) above a reference vegetated surface, such as a short fescue grass, are representative of the atmospheric boundary layer and are at equilibrium with the reference surface.

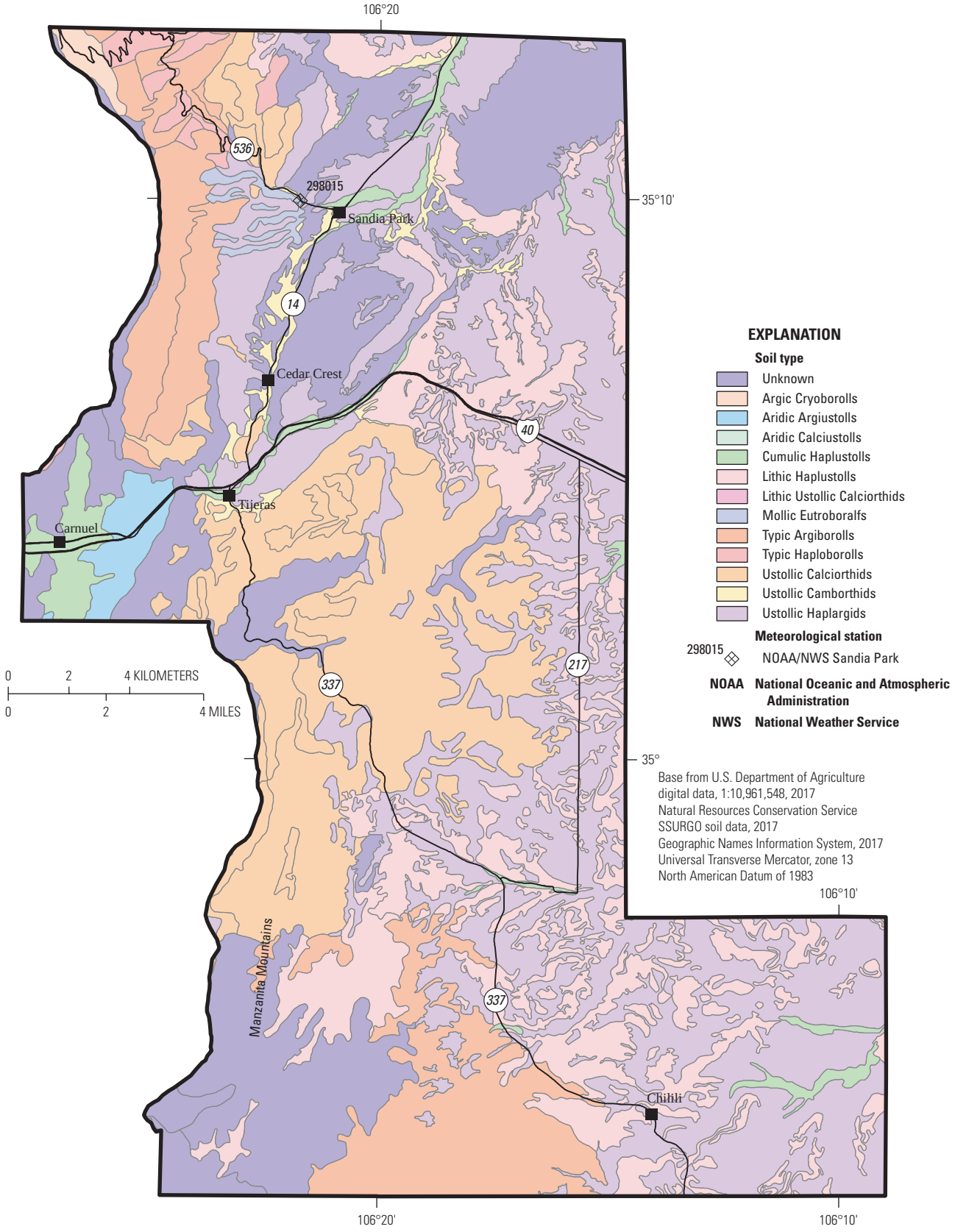

Figure 3. Soil types in the East Mountain area of Bernalillo County, New Mexico.

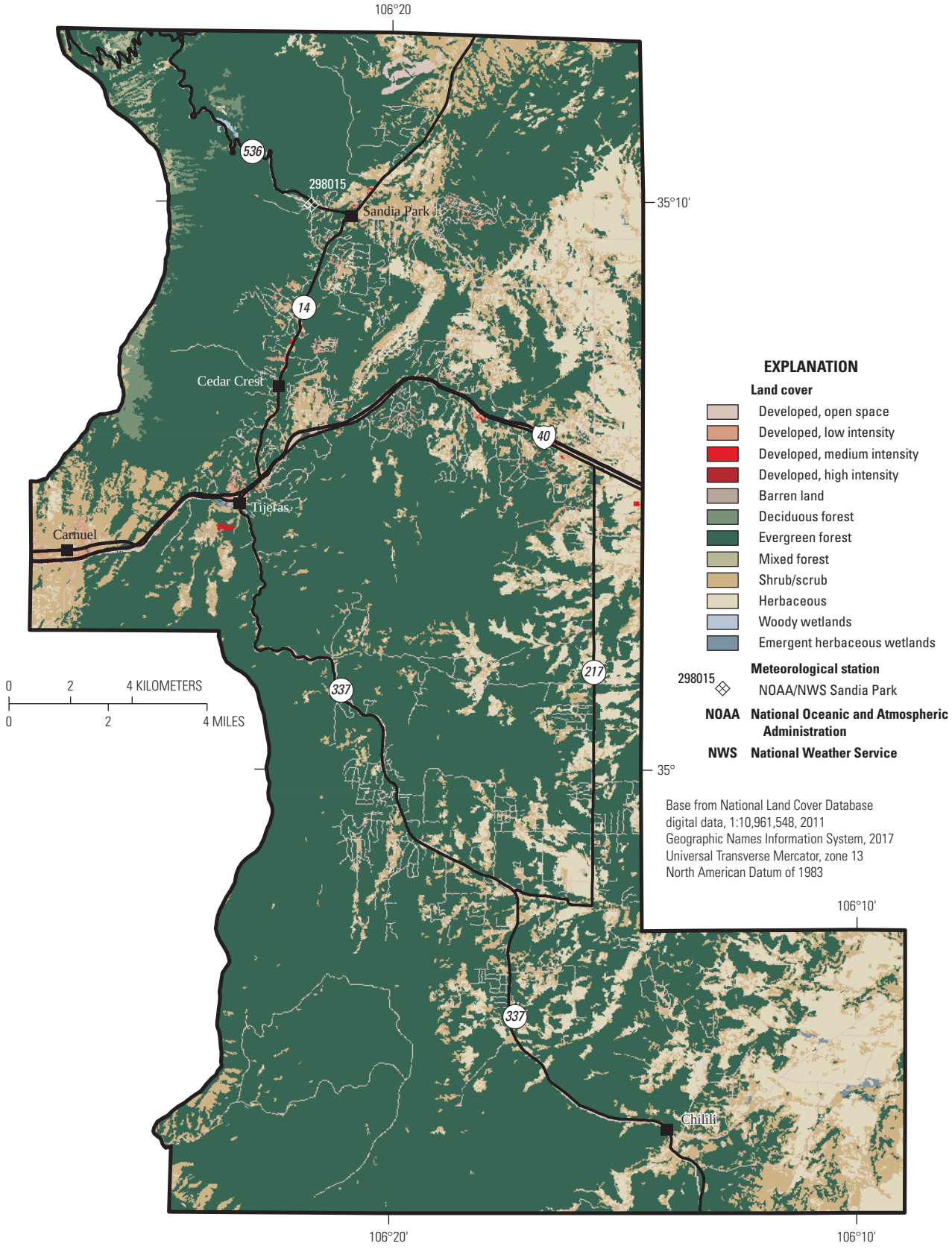

Figure 4. Land cover in the East Mountain area of Bernalillo County, New Mexico.

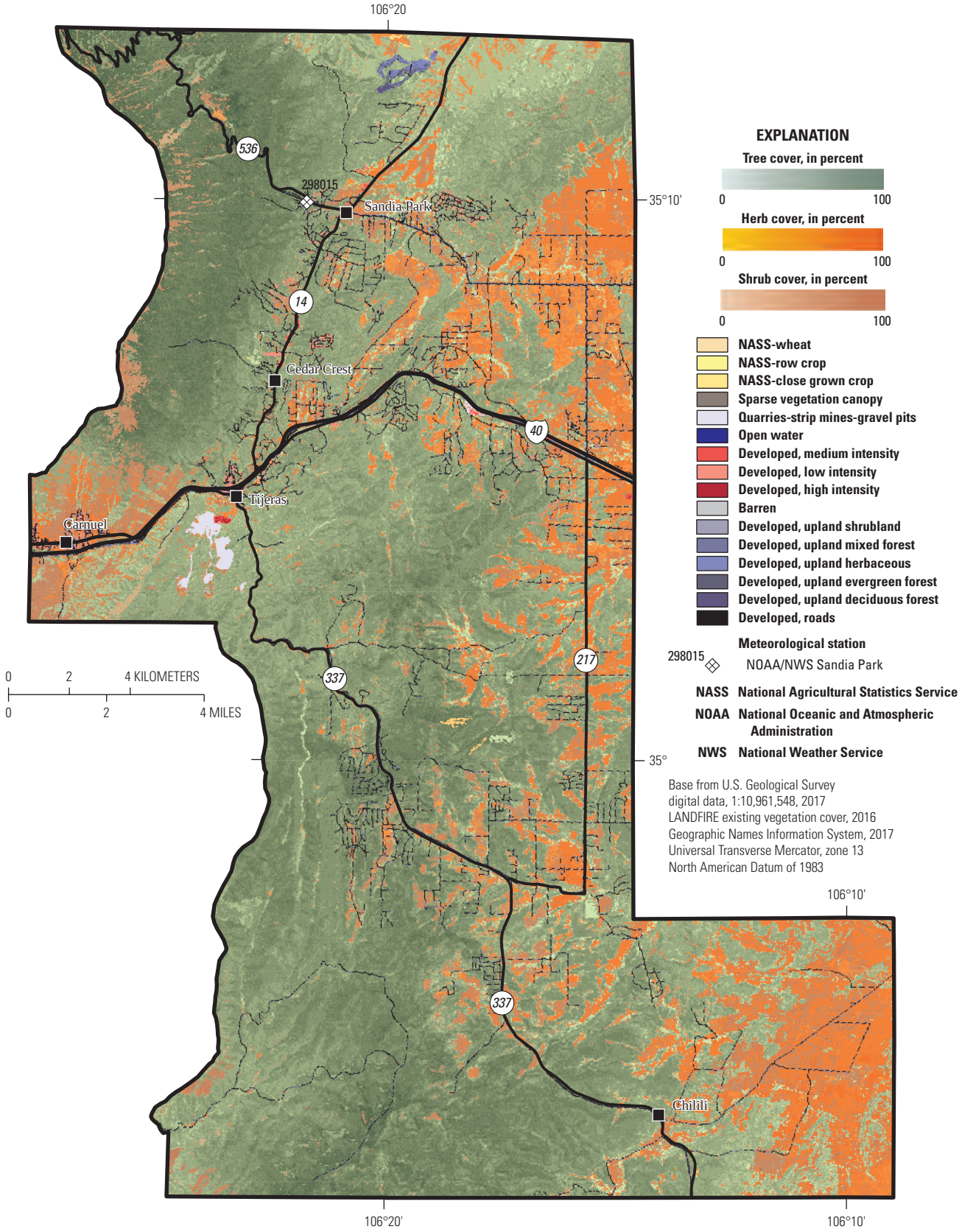

Figure 5. Vegetation cover in the East Mountain area of Bernalillo County, New Mexico.

Potential Evapotranspiration

Potential ET is a representation of the theoretical maximum ET from a vegetated surface under nonlimiting conditions. As a practical approximation of potential ET, reference ET (*ETo*) can be estimated for specific vegetated surface conditions. For example, *ETo* can be calculated for a reference surface using the standardized Penman-Monteith equation (Allen and others, 1998) using daily meteorological data:

$$ETo = \frac{0.408\,\Delta\left(Rn_d - G_d\right) + \gamma\,\frac{900}{Ta+273}u_2\left(e_s - e_a\right)}{\Delta + \gamma\left(1 + 0.34\,u_2\right)} \quad (1)$$

where

ETo is the reference ET, in millimeters per day;
Δ is the slope of the saturation vapor pressure temperature relation, in kilopascals per degree Celsius;
Rn_d is the daily net radiation flux density at the canopy surface, in megajoules per square meter per day;
G_d is the daily ground heat flux density, in megajoules per square meter per day;
γ is the psychrometric constant, in kilopascals per degree Celsius;
Ta is the daily mean air temperature at 2-m height, in degrees Celsius;
u_2 is the wind speed at 2-m height, in meters per second;
e_s is the saturation vapor pressure of air, in kilopascals; and
e_a is the vapor pressure of air, in kilopascals.

Allen and others (1998) define the reference surface as "a hypothetical reference crop with an assumed crop height of 0.12 m, a fixed surface resistance of 70 [seconds per meter] (s/m) and an albedo of 0.23," which generally describes a well-watered, mowed grass surface. Measurements of *Ta*, dew-point temperature (*Tdp*), u_2, Rn_d, and G_d are needed to calculate daily reference ET using equation 1.

Actual Evapotranspiration

Actual evapotranspiration (*ETa*) over a land surface with conditions that differ from the reference surface is estimated as a product of *ETo* and a time-varying crop coefficient (*Kc*, dimensionless). Allen and others (1998) provide an extensive list of *Kc* values for nonstressed, well-managed crops in subhumid climates, the latter characterized by a minimum relative humidity of approximately 45 percent and a u_2 of approximately 2 meters per second. A partial list of *Kc* values for vegetation types common to the East Mountain area is provided in table 1. More detail on application of crop coefficients, including within-season adjustments, is presented in Martin and Gilley (1993).

Remote Sensing Evapotranspiration Estimation

Several models have been developed that can use satellite data as a basis for ET estimation (Gowda and others, 2007). Some widely used examples include Surface Energy Balance Algorithm for Land (SEBAL; Bastiaanssen and others, 1998), Surface Energy Balance System (SEBS; Su, 2002), Mapping EvapoTranspiration at high Resolution and with Internalized Calibration (METRIC; Allen and others, 2007), and Operational Simplified Surface Energy Balance (SSEBop;

Table 1. Crop coefficients (*Kc*) for use with the Penman-Monteith reference evaporation (*ETo*) equation to estimate actual evapotranspiration (*ETa*).

[m, meter]

Crop	*Kc*[1]			Maximum crop height (m)
	Initial	Midseason	End	
Pasture, rotational grazing	0.40	0.85–1.05	0.85	0.15–0.30
Pasture, extensive grazing	0.30	0.75	0.75	0.10
Turf grass, cool season	0.90	0.95	0.95	0.10
Turf grass, warm season	0.80	0.85	0.85	0.10
Conifer trees[2]	1.00	1.00	1.00	10

[1]From Allen and others (1998).

[2]If well-watered conditions do not exist, *Kc* for conifers may be less than values presented.

Senay and others, 2013). A general approach used by these and other remote-sensing-based models is to determine ET as a residual of the land-surface energy balance equation:

$$\lambda ET = LE = RN - G - H \quad (2)$$

where

- λ is the latent heat of vaporization, ~2.45 megajoules per kilogram;
- ET is evapotranspiration, in millimeters per day;
- LE is the latent heat flux density, in watts per square meter;
- Rn is the net radiation flux density, in watts per square meter;
- G is the ground heat flux density, in watts per square meter; and
- H is the sensible heat flux density, in watts per square meter.

Equation 2 is solved using a combination of satellite measurements of surface reflectance and surface temperature, along with energy-balance parameters derived from ground-based meteorological data. Additional details are provided herein for the SSEBop model, which was the remote-sensing ET model applied in this study.

Materials and Methods

This section describes the models and data used to evaluate the landscape and climatic influences on actual evapotranspiration. Analysis methods used also are described.

Parameter-Elevation Regressions on Independent Slopes Model (PRISM)

PRISM (Daly and others, 2000, 2008) is a commonly used suite of gridded, spatial climate data products developed from a wide range of climate monitoring networks (Schneider and Ford, 2011; Wang and others, 2006). The PRISM products were created to address spatially sparse location climatology (Daly, 2006; Daly and others, 2008) by generating spatially and temporally continuous climate data throughout the contiguous United States. PRISM uses data from land-based weather stations, digital elevation models, and other spatial datasets, and interpolates between stations using local regression-fit curves as linear functions of elevation. Monthly P data are available at 4-kilometer (km) resolution. A strength of PRISM is that it accounts for geospatially varying effects on P, such as terrain-induced climatic gradation (Daly, 2006). A key model assumption is that station data are at a high enough resolution to capture coarse-scale climatic effects, and that elevation is the primary factor governing finer-scale distribution of P (Daly and others, 2008).

SSEBop Model

The SSEBop model (Senay and others, 2013, 2016) was used to estimate *ETa* in the study area. SSEBop is a geospatial ET estimation model that uses spatially variable, remotely sensed, thermal land-surface data to adjust temporally variable *ETo* values to derive spatiotemporally variable estimates of *ETa* across a study area. Data used to parameterize the SSEBop model are summarized in table 2. Parameterization closely followed the methods used by Senay and others (2016) when they applied SSEBop to the Colorado River Basin.

Table 2. Summary of data used to parameterize the Operational Simplified Surface Energy Balance (SSEBop) Model.

[m, meter; TIR, thermal infrared; NDVI, Normalized Difference Vegetation Index; VNIR, visible and near-infrared; MODIS, moderate Resolution Imaging Spectroradiometer; ET, evapotranspiration; GDAS, Global Data Assimilation System; SRTM, Shuttle Radar Topography Mission; NA, not applicable]

Dataset	Frequency	Resolution (m)	Date source and reference
Land surface temperature (*Ts*)	16-day	100	Landsat 8 (TIR); Irons and others (2012)
NDVI	Monthly	100	Landsat 8 (VNIR); Irons and others (2012)
Albedo (α)	16-day	1,000	MODIS (MCD43B3); Schaaf and others (2002)
Reference ET (*ETo*)	Daily	10,000	GDAS; Senay and others (2007)
Maximum air temperature (*Ta*)	Daily	1,000	Daymet; Thornton and others (2014)
Average net radiation (*Rn*)	Daily	1,000	Daymet; Thornton and others (2014)
Elevation	NA	30	SRTM; Farr and Kobrick (2000)

Both Landsat 8 and Landsat 7 Enhanced Thematic Mapper Plus (ETM+) multispectral data were used for all days that met a scene cloud threshold of 60 percent or less. Landsat 8 red band 4 (0.636–0.673 micrometer [μm]) and near-infrared band 5 (0.851–0.879 μm) and Landsat 7 ETM+ red band 3 (0.63–0.69 μm) and near-infrared band 4 (0.77–0.90 μm) were used to calculate the Normalized Difference Vegetation Index (NDVI). Thermal-infrared data from Landsat 8 band 10 (10.60–11.19 μm) and Landsat 7 ETM+ band 6 (10.40–12.50 μm) were used to calculate land-surface temperature (*Ts*) using NDVI-based emissivity calculation procedures (Sobrino and others, 2004; Senay and others, 2016). The *ETo* was calculated using the standardized Penman-Monteith equation (eq. 1) using data from a gridded surface meteorological dataset called GRIDMET (Abatzoglou, 2013).

Methods used to calculate *ETa* are described in Senay (2018) and Senay and others (2013, 2016, 2017) and will be presented briefly here. Rather than solve all the energy balance terms (eq. 2), SSEBop applies several simplifications based on clear-sky net radiation balance principles. *ETa* for each Landsat pixel and time is estimated using equation 3 as a fraction of *ETo*:

$$ETa = f_{ET}(k\ ETo) \tag{3}$$

where

- ETa is the actual ET, in millimeters per day;
- f_{ET} is the ET fraction, unitless;
- k is a coefficient used to scale reference ET to maximum ET of given land use, unitless (k = 1.25 used in this study); and
- ETo is the grass reference ET, in millimeters per day.

Satellite data are used to define the f_{ET} term using equation 4:

$$f_{ET} = 1 - (Ts - Tc) / dT \tag{4}$$

where

- Ts is the satellite-observed land-surface temperature for given pixel and time, in Kelvin;
- dT is the differential temperature representing the difference between the hot and cold pixel ($Th - Tc$), in Kelvin;
- Th is the estimated Ts at the idealized "hot/dry" condition for given pixel and time, in Kelvin; and
- Tc is the estimated Ts at the idealized "cold/wet" condition for given pixel and time, in Kelvin.

The *Th* for each pixel and time represents the maximum land-surface temperature that occurs under dry limiting conditions (and minimal ET). The *Tc* for each pixel and time represents the minimum land-surface temperature that occurs under wet limiting conditions (and maximal ET). Senay and others (2007) assume the fraction of ET that occurs at a given pixel can be linearly interpolated between *Th* and *Tc* according to *Ts*.

Senay and others (2013) develop the rationale for assuming that *Tc* can be estimated as a fraction of air temperature (eq. 5), and *Th* can be estimated by adding a generalized temperature difference (eq. 6) to *Tc* (eq. 7):

$$Tc = c\ Ta \tag{5}$$

$$dT = Rn^{*}\ r_{ah} / \rho\ Cp \tag{6}$$

$$Th = Tc + dT \tag{7}$$

where

- c is a correction factor, unitless (ranging from 0.97 to 0.99 in this study; Senay and others, 2016, 2017);
- Rn^{*} is the daily mean clear-sky net radiation flux density, in Joules per square meter second;
- r_{ah} is the aerodynamic resistance to heat flow from a hypothetical bare and dry surface, in seconds per meter (110 s/m in this study; Senay and others, 2013, 2016);
- ρ is the density of air, in kilograms per cubic meter; and
- Cp is the specific heat of air at constant pressure (1,013 Joules per kilogram Kelvin).

The relation between *Tc* and *Ta* (eq. 5) was calculated for each Landsat image to capture spatial and temporal variations and was found to vary between 0.97 and 0.99 for most cases (Senay and others, 2017). The value of r_{ah} (110 s/m) was calculated using a rearranged equation 6 with eddy covariance ET data from 45 stations throughout the United States (Senay and others, 2013, 2016). The parameterization used in this study assumes that *dT* is based on clear-sky conditions (and thus can use *Rn**), because the thermal remote sensing data primarily are from clear-sky conditions, and thus *dT* is unique for each day and location but does not change from year to year. These assumptions allow equation 4 to be solved for each day and pixel using only *Ts*, which is determined from satellite data, and *Ta*, which is determined from climatic data.

Like other remote-sensing methods, SSEBop has uncertainty in its estimation of *ETa*. An assessment of SSEBop (1-km resolution) uncertainty used data from 42 eddy-covariance flux towers across the United States (cropland, grassland, forest, shrubland, and woody savanna) from 2001–2007 aggregated to daily and monthly time scales (Chen and others, 2016). They found relative errors <20 percent for monthly *ETa* estimates. Uncertainty in SSEBop (1-km resolution) estimation of annual mean *ETa* on a mixed agricultural landscape in East Africa was less than 12 percent (Alemayehu and others, 2017). Preliminary validation of SSEBop (100-m resolution) simulated *ETa*

compared to eddy-covariance flux tower observed *ETa* data collected from 2007 to 2014 in New Mexico yielded coefficient of determination (R^2) values ranging from 0.41 to 0.75 at six native-vegetation sites (juniper savannah, pinyon juniper, ponderosa pine, spruce fir pine, Chihuahuan creosote shrubland, and Chihuahuan grassland) on overpass days and much higher R^2 (>0.7) at monthly time scales (Senay and others, 2019). It is expected that SSEBop (100-m resolution) *ETa* data used in this report fall within similar ranges of uncertainty. Overall, these results indicate that the monthly *ETa* data used in this study provide ET estimates that are reasonably accurate, are representative of the native vegetation species common to the region, and are at an appropriate timescale for water budget analyses.

Data for the East Mountain Area

Geospatial datasets describing atmospheric, topographic, soil, and vegetation characteristics in the East Mountain area were compiled, and variables from these datasets were compared to 2015 SSEBop *ETa* estimates to characterize factors influencing ET in the study area (fig. 1), as summarized in table 3. Each geospatial dataset was reclassified and standardized to match the 100-m pixel resolution of the *ETa* datasets. Data for each raster were extracted using the "Sample" tool in geographic information system (GIS) software ArcMap 10.5.1 (Esri, 2017), where each raster was entered as an input with the location of extraction being the pixel centroid in the annual *ETa* dataset. At maximum, data for 773,414 cells (100-m resolution) were extracted for each dataset. This method has two limitations. First, some datasets contained empty pixels, which may have biased the results, depending on the distribution of those pixels; the effect of this bias was not assessed. Second, the sampling procedure created a scale mismatch, whereby the 100-m *ETa* pixel was compared to characteristics at different scales for several variables (for example, NDVI at 30-m resolution, leaf area index (LAI) at 300-m resolution); again, the effect of this bias was not assessed.

Data used in the analysis included *ETa* from SSEBop; precipitation from PRISM (*P*); longitude, latitude, elevation, slope, aspect and albedo from the Web Soil Survey (WSS); land-cover type and tree canopy percentage from the U.S. Forest Service National Land Cover Database (NLCD); LAI from the Project for On-Board Autonomy-Vegetation (PROBA-V); NDVI created from an existing vegetation cover dataset from the USGS Earth Resources Observation and Science (EROS) Center; and soil parameters, including depth to bedrock or impermeable layer, available water storage (0–100 cm and 0–25 cm), and soil layer 1 depth from WSS and available water capacity, bulk density, soil erodibility, and sand, silt, and clay fractions from NRCS Soil Survey Geographic (SSURGO) data (table 3). Analyses in this report will refer to the specific variable names defined in table 3.

Tree canopy percentages were determined by the U.S. Forest Service using methods from Huang and others (2001). Reference data for tree canopy density were derived from high-spatial-resolution (1-m) digital orthophoto quadrangle images overlain on 30-m Landsat 7 ETM+ grids to calculate the percentage of 1-m canopy pixels within each 30-m grid. These reference data were used to develop canopy density models that related reference tree canopy density to ETM+ spectral band data (using all seven bands and spanning 0.45–12.50 μm). These models were extrapolated spatially to develop a complete national NLCD coverage of 30-m resolution tree canopy density. The ETM+ data used to develop the 2011 NLCD coverage (table 3) were collected at a 30-m spatial resolution during the spring and summer months of 2011.

LAI data were produced by Copernicus Global Land Service (2017) using methods described by Baret and others (2013) and Verger and others (2015). LAI is defined as half the total area of green elements of the canopy (so as to account for just one side of the leaves) per unit horizontal ground area. These LAI data were generated using a neural network to process top-of-canopy reflectance in the red (0.61–0.68 μm), near-infrared (0.78–0.89 μm), and short-wave infrared (1.58–1.75 μm) bands from the Vegetation multispectral sensor aboard the Satellite Pour l'Observation de la Terre satellite (SPOT–4). The satellite-derived value accounts for all canopy layers, including the understory, which may represent a very significant contribution, particularly for forests. Practically, the LAI quantifies the effective number of leaf layers of the vegetation cover. The data were reported at a 300-m spatial resolution and were mean values reported for 2015 (table 3).

NDVI data were created using 30-m-resolution red and near-infrared bands from a Landsat 8 overpass image in July 2017, obtained from the USGS Landfire database (Wildland Fire Science, EROS, 2016). The Landsat 8 imagery was processed using the image analysis toolbar (ArcMap 10.5.1, Esri, 2017) with NDVI values ranging from −1 to 1.

Table 3. Summary of data used to assess spatial variability of evapotranspiration in the East Mountain area, Bernalillo County, New Mexico.

[Dataset variable name: ETa1-ETa12, monthly actual evapotranspiration for January (1) through December (12); ETa2015, annual total *ETa* for 2015; P1-P12, monthly precipitation for January (1) through December (12); P2015, annual total P for 2015. Source: SSEBop, Simplified Surface Energy Balance Operationalized; PRISM, Parameter-elevation Regressions on Independent Slopes Model; NAVD 88, North American Vertical Datum of 1988; NRCS, Natural Resources Conservation Service; WSS, Web Soil Survey; SSURGO, Soil Survey Geographic; NLCD, National Land Cover Database; PROBA-V, Project for On-Board Autonomy-Vegetation; LF, Landfire. Unit of measure: m, meter; km, kilometer; cm, centimeter. Miscellaneous: NA, not applicable; %, percent; var., variable]

Dataset		Data-collection period	Resolution	Data source and reference
Description	Variable name			
Atmospheric				
Actual evapotranspiration	ETa1-ETa12, ETa2015	Monthly, annual	100 m	SSEBop; Senay and others (2019)
Precipitation	P1-P12, P2015	Monthly, annual	4 km	PRISM; PRISM Climate Group (2017)
Topography				
Elevation (m NAVD 88)	Elevation	NA	100 m	WSS; Soil Survey Staff, NRCS (2017)
Slope (%)	Slope	NA	100 m	WSS; Soil Survey Staff, NRCS (2017)
Aspect: eastness, northness	Eastness, Northness	NA	100 m	WSS; Soil Survey Staff, NRCS (2017)
Soil				
Available water storage, depth-weighted mean (0–100 cm)	AWatSt100	NA	Variable	WSS; Soil Survey Staff, NRCS (2017)
Available water storage, depth-weighted mean (0–25 cm)	AWatSt025	NA	Variable	WSS; Soil Survey Staff, NRCS (2017)
Depth of soil layer 1 (cm)	SoilZ1	NA	Variable	WSS; Soil Survey Staff, NRCS (2017)
Depth of soil to bedrock or impermeable layer	SoilZMx	NA	Variable	WSS; Soil Survey Staff, NRCS (2017)
Soil particle size	PartSize	NA	Variable	SSURGO; Soil Survey Staff, NRCS (2012)
Available water capacity of soil layer 1 (fraction)	AWC1	NA	Variable	SSURGO; Soil Survey Staff, NRCS (2012)
Clay content of soil layer 1 (%)	Clay1	NA	Variable	SSURGO; Soil Survey Staff, NRCS (2012)
Sand content of soil layer 1 (%)	Sand1	NA	Variable	SSURGO; Soil Survey Staff, NRCS (2012)
Silt content of soil layer 1 (%)	Silt1	NA	Variable	SSURGO; Soil Survey Staff, NRCS (2012)
Bulk density of soil layer 1 (%)	SoilBD1	NA	Variable	SSURGO; Soil Survey Staff, NRCS (2012)
Soil erodibility of soil layer 1	SoilK1	NA	Variable	SSURGO; Soil Survey Staff, NRCS (2012)
Vegetation				
Land-cover type	LandcoverType	2011	30 m	NLCD; Homer and others (2015)
Tree canopy, percent	TreeCanopy	2011	30 m	NLCD; Homer and others (2015)
Leaf area index	LAI	2015	300 m	PROBA-V; Copernicus Global Land Service (2017)
Normalized Difference Vegetation Index	NDVI	Spring, Summer	30 m	EVC; Wildland Fire Science, Earth Resources Observation and Science Center (2016)
Albedo (fraction)	Albedo	Variable	100 m	WSS; Soil Survey Staff, NRCS (2017)
Existing vegetative cover	EVC	Spring, Summer	30 m	LF: Wildland Fire Science, Earth Resources Observation and Science Center (2016)

Data Analysis

The *ETa* dataset contained n = 773,414 pixels, but some study-area characteristics were undefined for some pixels, which reduced n for some models. Regression analyses and statistical analyses were determined at the spatial resolution of the *ETa* data (100 m, n = 773,414 pixels). Datasets containing less than 773,414 pixels either had missing values in the original dataset (tables 4 and 5, "NA") or had values removed for quality control (tables 4 and 5, "Removed"). As an example of data quality control where values were corrected but not removed, SoilK1 values of 101.6228 percent (9,232 total) were corrected to 100 percent because this value represents the percentage of erodible soil, and a value greater than 100 percent is not possible. Furthermore, using a graphical comparison method and correlation analyses, comparing these pixels (101.6228 percent) to other pixels with very high percentages of erodible soil indicated that these pixels were most likely meant to have values of 100 percent. Aspect (degrees) data were converted to Northness and Eastness (fractions), allowing for inclusion of aspect in parametric statistical tests and modelling.

$$\text{Northness} = \cos\ [(\text{aspect}] * 3.14159 / 180) \quad (8)$$

$$\text{Eastness} = \sin\ [(\text{aspect}] * 3.14159 / 180) \quad (9)$$

For example, the four cardinal aspect directions (aspects facing north, east, south, and west) would translate into Northness values of 1, 0, −1, and 0, and Eastness values of 0, 1, 0, and −1, respectively.

ETa and *P – ETa*, also called "available water" (water that is available for soil water storage, streamflow, groundwater recharge, and other ecosystem functions), were analyzed at both annual and monthly scales and related to topography, soil, and vegetation data from the East Mountain area of New Mexico (table 3). The relation between each predictor variable and the two response variables, *ETa* and *P – ETa*, at both annual and monthly scales, was characterized using linear regression and descriptive statistics. Continuous (table 4) and categorical (table 5) datasets were analyzed to better characterize the study area and understand their relations with *ETa* and available water. Regression slope (m), intercept (b), Pearson's r, I, and R^2 were determined for each linear model, and t-tests (Helsel and Hirsch, 2002) were used to test the null hypothesis that the slope of the predictor variable versus the response variable equaled zero, with a probability (p) < 0.05 indicating a slope significantly different from zero.

A parametric one-way analysis of variance (ANOVA) test (Helsel and Hirsch, 2002) was performed on categorical datasets of table 5 to determine whether grouped annual *ETa* datasets differed. The parametric test was used, because each analyzed dataset met parametric assumptions such as category sizes being greater than 30 samples. The F-statistic (F), denominator degrees of freedom (denom df), degrees of freedom (df), and p values were determined for each dataset. One-way ANOVA p values were used to test the null hypothesis that annual *ETa* mean values were equal in each category within a dataset, with $p < 0.05$ indicating a significant difference between *ETa* values in two or more categories. A parametric multiple comparison test (Helsel and Hirsch, 2002) was then performed to determine which specific categories had different mean *ETa* values. In this test, $p < 0.05$ indicates a difference between mean *ETa* values of specific category pairings (for example, evergreen forest and deciduous forest).

Boxplots were created to show central tendency and variability of *ETa* and *P – ETa* within subcategories of variables identified as having notable correlations by the regression analysis. Boxplots of annual *ETa* and *P – ETa* were developed to compare and contrast *ETa* and *P – ETa* across five natural land-cover types (evergreen forest, shrub, herbaceous, deciduous forest, and mixed forest) and four developed land-cover types. Developed land-cover categories were defined by percentage of impervious area: open space (developed open, <20 percent), low-intensity developed (developed low, 20–49 percent), medium-intensity developed (developed medium, 50–79 percent), and high-intensity developed (developed high, >79 percent). Variability within each land-cover type was further analyzed by grouping annual *ETa* and *P – ETa* into elevation, tree canopy percentage, and soil texture categories.

Table 4. Statistical summary of continuous data used to assess spatial variability of actual evapotranspiration (*ETa*) and available water in the East Mountain area, Bernalillo County, New Mexico.

[Refer to table 3 for dataset variable names and more detailed information about each dataset. All statistics were generated using a 100-meter pixel size. min, minimum value; Q1, value of first quartile; Q3, value of third quartile; max, maximum value; not applicable, data points missing from original dataset; removed, removed from the dataset during quality control; LAI, leaf area index; NDVI, Normalized Difference Vegetation Index]

Variable name, units	Min	Q1	Median	Mean	Q3	Max	Number of values		
							Not applicable	Removed	In final dataset
ETa									
ETa2015, millimeters	79	396	547	543	675	1,335	8,881	0	764,533
ETa1, millimeters	0	0	3	8	11	62	6,290	0	767,124
ETa2, millimeters	0	0	15	19	33	87	6,262	0	767,152
ETa3, millimeters	0	3	15	20	33	139	5,443	0	767,971
ETa4, millimeters	0	10	36	38	61	167	6,622	0	766,792
ETa5, millimeters	0	47	70	67	89	171	5,081	0	768,333
ETa6, millimeters	0	49	73	73	97	197	4,876	0	768,538
ETa7, millimeters	0	99	112	109	124	198	6,233	0	767,181
ETa8, millimeters	0	73	93	90	108	176	5,353	0	768,061
ETa9, millimeters	0	27	46	46	64	136	6,519	0	766,895
ETa10, millimeters	0	5	15	18	28	101	6,572	0	766,842
ETa11, millimeters	0	13	21	23	33	77	6,393	0	767,021
ETa12, millimeters	0	14	28	30	47	68	6,470	0	766,944
Precipitation									
P2015, millimeters	0	566	607	608	639	772	1,384	1	772,030
P1, millimeters	0	33	37	38	39	81	1,643	1	771,771
P2, millimeters	20	31	32	33	36	55	2,605	111	770,809
P3, millimeters	0	21	23	25	24	62	1,641	1	771,773
P4, millimeters	0	16	17	17	18	21	2,014	0	771,400
P5, millimeters	0	62	73	72	81	91	2,320	1	771,094
P6, millimeters	0	31	32	34	36	53	2,529	0	770,885
P7, millimeters	94	126	136	134	143	161	2,605	263	770,809
P8, millimeters	32	35	40	43	49	76	2,605	62	770,809
P9, millimeters	16	27	29	29	32	46	2,605	73	770,809
P10, millimeters	60	72	82	88	96	165	2,605	957	770,809
P11, millimeters	0	27	30	31	34	59	300,292	0	473,122
P12, millimeters	0	48	60	60	70	93	2,567	18	770,847
Topography									
Elevation, meters	1,752	2,080	2,157	2,182	2,250	3,254	4,210	0	769,204
Slope, degrees	0	7	13	22.87	43	75	2,350	0	771,064
Northness, fraction	−1	–0.71	0	0	0.71	1	61,809	57,657	711,605
Eastness, fraction	–1	–0.32	0.24	0.19	0.88	1	61,809	57,657	711,605

Table 4. Statistical summary of continuous data used to assess spatial variability of actual evapotranspiration (*ETa*) and available water in the East Mountain area, Bernalillo County, New Mexico.—Continued

[Refer to table 3 for dataset variable names and more detailed information about each dataset. All statistics were generated using a 100-meter pixel size. min, minimum value; Q1, value of first quartile; Q3, value of third quartile; max, maximum value; not applicable, data points missing from original dataset; removed, removed from the dataset during quality control; LAI, leaf area index; NDVI, Normalized Difference Vegetation Index]

Variable name, units	Min	Q1	Median	Mean	Q3	Max	Number of values		
							Not applicable	Removed	In final dataset
Soil									
SoilZ1, centimeters	0	130	180	408.3	200	1,520	3,202	54	770,212
Clay1, percent	0	16.0	17.0	15.05	20.5	31.5	2,346	35	771,068
Silt1, percent	0	22.7	37.3	27.69	37.9	54.8	2,579	0	770,835
Sand1, percent	0	21.7	42.0	38.28	59.7	65.9	2,587	0	770,827
SoilK1, percent	0	33.01	33.01	27.56	33.01	100	2,585	0	770,829
AWC1, fraction	0	0.09	0.15	0.1158	0.15	0.20	2,547	0	770,867
SoilBD1, percent	1.2	1.2	1.4	1.32	1.4	1.4	148,691	146,116	624,723
SoilZMx, centimeters	380	860	1,520	1,180	1,520	1,520	1,975	0	771,439
AWatSt025, centimeters	0	2.84	3.88	3.51	4.19	5.00	2,605	1,460	770,809
AWatSt100, centimeters	0	5.63	8.49	10.35	16.55	20.00	1,330	186	772,084
Vegetation									
TreeCanopy, percent	0	18	30	29.62	42	72	2,536	274	770,878
LAI, percent	0	11	19	19.32	26	46	2,446	185	770,968
NDVI, ratio	–0.1892	0.0196	0.1045	0.115	0.2	1	3,078	0	770,336
Albedo, fraction	0	0.16	0.21	0.21	0.23	0.30	1,763	0	771,651

Table 5. Statistical summary of categorical data used to assess spatial variability of actual evapotranspiration (*ETa*) and available water in the East Mountain area, Bernalillo County, New Mexico.

[Refer to table 3 for dataset variable names and more detailed information about each dataset. not applicable, data points missing from original dataset; removed, removed from the dataset during quality control]

Variable name	Number of values		
	Not applicable	Removed	In final dataset
LandcoverType	3,892	44	769,522
PartSize	1,963	212	771,451

Multiple linear regression *ETa* models (annual and monthly) were developed using the stepwise method with annual or monthly *ETa* (from SSEBop) as the dependent variable and topographic, vegetation, soil, and climate characteristics as independent variables. The R programming language stepwise method, specifically the "step" function, with "both" (forward and backward) selected as the direction of stepwise search, was used to determine the best multivariate linear model (R Core Team, 2017); R x64 version 3.4.0 was used in this study. This selection criterion allows the function to add and subtract variables from the model as it searches for the set of variables having the lowest Akaike information criterion (AIC) (Akaike, 1974). AIC estimates the relative quality of statistical models for a provided dataset, accounting for tradeoffs between the goodness of fit and the complexity of the model by rewarding goodness of fit as assessed by the likelihood function, while also penalizing any increase in the number of predictor variables. The penalty discourages overfitting the model, because increasing the number of model parameters almost always improves the goodness of fit. The formula for computing the AIC is as follows:

$$AIC = 2a - 2\ln\left(\hat{L}\right) \tag{10}$$

where

a is the number of estimated parameters in model; and

$\hat{L}$ is the maximum value of likelihood function for model (Aho and others, 2014).

All datasets from table 4 except monthly *ETa* and *P* were included in the model selection process. Monthly *ETa* datasets were excluded because of their extensive cross-correlation with annual *ETa*. Monthly *P* was excluded because changes to *ETa* are the result of ponding and soil moisture storage, rather than *P* specifically. Furthermore, spatiotemporal variability of East Mountain area *P* is extensive, as discussed below, and characterizing the age of precipitation water that is evaporated was beyond the scope of this study. Annual *P* was included because the aggregate of *P* for the entire year best represented locations within the East Mountain area where the most water was available for annual *ETa*.

Climate in the East Mountain Area for the Study Period, 2015

Precipitation averaged 617.4 millimeters (mm) in the East Mountain area during the study period (2015) (table 6). The study period was about 132 mm (27 percent) wetter and 0.7 °C warmer than the most recent 30-year climate normal period (1981–2010) for the East Mountain area (table 6). On a monthly basis, May (+148 percent), July (+92 percent), October (+103 percent), and December (+61 percent) had considerably more P in 2015 than the mean for the 30-year period. March, April, August, and September all had 36–45 percent less P in 2015 than during the climate normal period. February, March, June, September, and October averaged greater than (>) 1 °C above normal, and only May averaged >1 °C below normal across the area, the remaining months were within 1 °C of normal. These patterns are for the East Mountain area as a whole, and considerable spatial climatic variation within the area is expected for P and temperature, as well as the response of *ETa* to those climatic conditions. Also, values for monthly and annual P in table 6 differ slightly from those in table 4; data from table 6 were aggregated from all 4-km PRISM cells that overlaid the East Mountain area, whereas table 4 subdivided the 4-km cells into 100-m cells and aggregated all 100-m cells that overlaid the East Mountain area, causing a slight difference between values in these tables. All subsequent analyses in this report use data from table 4.

Table 6. Spatially averaged precipitation and mean air temperature for the study period (2015) and the most recent climate normal period (1981–2010) from Parameter-Elevation Regressions on Independent Slopes Model (PRISM) for the East Mountain area, Bernalillo County, New Mexico.

[mm, millimeter; °C, degrees Celsius; NA, not applicable]

Month	Precipitation (mm)		Mean temperature (°C)	
	2015	1981–2010	2015	1981–2010
January	39.4	29.1	−0.1	−0.5
February	34.0	32.0	3.2	1.3
March	25.4	39.7	6.3	4.6
April	17.6	32.0	8.7	8.6
May	73.4	29.6	11.8	13.6
June	33.3	24.8	20.0	18.5
July	133.0	69.3	19.9	20.5
August	45.6	73.9	20.3	19.4
September	29.6	49.9	18.1	16.0
October	91.8	45.2	12.2	10.2
November	32.2	21.6	4.1	4.2
December	62.1	38.5	−0.2	−0.5
Total	617.4	485.5	NA	NA
Mean	NA	NA	10.4	9.7

ETa and Available Water in the East Mountain Area

Annual median *ETa* was 547 mm across the East Mountain area in 2015 (table 4). Monthly median *ETa* ranged from 3 mm in January to 112 mm in July, with 79 percent of annual *ETa* occurring from April to September and 51 percent occurring from June to August (table 4, fig. 6*A*). Interquartile range (third quartile [Q3] minus first quartile [Q1], table 4, fig. 6*A*) of monthly *ETa*, which indicates the middle 50 percent of *ETa* values in the East Mountain area, averaged 32 mm and ranged from 11 mm in January to 51 mm in April). Interquartile range expressed as a percentage relative to the median *ETa* indicates relative consistency in *ETa* within the East Mountain area in July (half the pixels were within ±11 percent of the median) as well as the other months from May through September (±20–40 percent). January through April and December had high relative variability in *ETa*, with interquartile ranges exceeding the median *ETa* for these months.

Annual median *P* was 607 mm across the East Mountain area in 2015 (table 4). Monthly median *P* ranged from 17 mm for April to 136 mm for July, with 54 percent of annual *P* occurring from April to September, 34 percent occurring from June to August, and 47 percent occurring during the monsoon season from July to October (table 4, fig. 6*B*). The interquartile range of monthly *P* averaged 11 mm and ranged from 2 mm for April to 24 mm for October. Interquartile range expressed as a percentage relative to the median *P* indicates

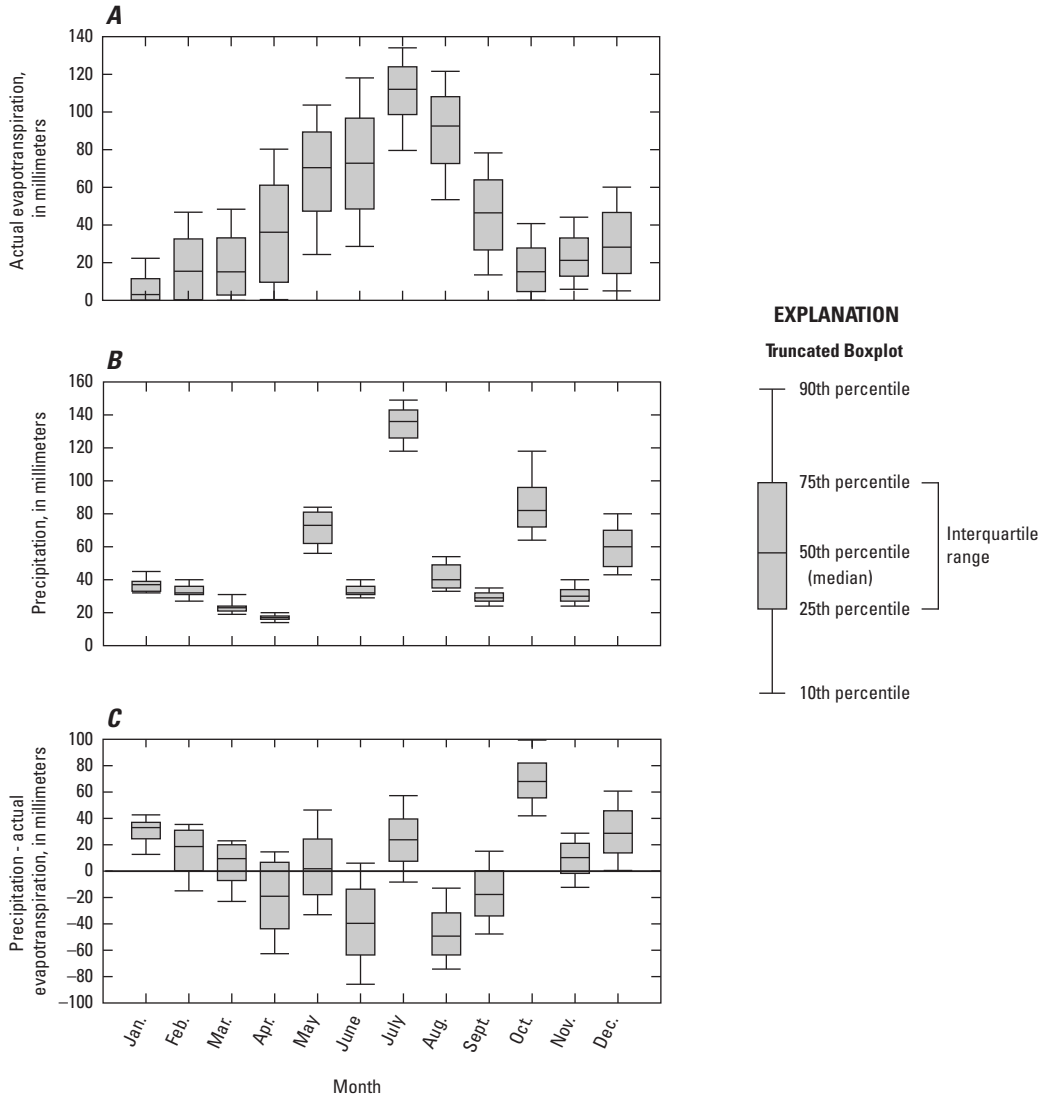

Figure 6. Monthly *A*, actual evapotranspiration (*ETa*), *B*, precipitation (*P*), and *C*, available water (*P* – *ETa*) distributions across 100-meter pixels in the East Mountain area of Bernalillo County, New Mexico, 2015.

that variability in *P* tended to increase with monthly median *P*, ranging from 12 percent for months with <25 mm, 18 percent for months with 25 to 40 mm, and 32 percent for months with at least 40 mm, excluding the largest rainfall month, July (median = 136 mm), which had a fairly uniform relative interquartile range of 13 percent.

Available water for the East Mountain area as a whole, expressed as median *P* minus median *ETa* from table 4, was 60 mm for 2015. Available water was negative (*P* < *ETa*) for April, June, August, and September (fig. 6*C*), which indicates that ET depleted soil water resources during those months. The remaining months had positive available water (*P* > *ETa*) ranging from 3 mm in May to 67 mm in October (fig. 6*C*). This monthly water-balance analysis did not differentiate whether the surplus available water contributed to runoff, increased soil water storage, or added to groundwater recharge.

High *P* amounts in the East Mountain area in May, July, and October (fig. 6*B*) were likely sufficient to generate surface runoff or increase soil moisture content. *P* – *ETa* values (fig. 6*C*) during these months illustrate how available water may have increased. In contrast, the negative median *P* – *ETa* values during the months of April, June, August, and September indicate that less water likely was available for ET. For example, one reason that median June *ETa* was only slightly higher than May *ETa* (fig. 6*A*) may be soil-moisture limitation from low *P* and negative *P* – *ETa*. In contrast, median monthly *ETa* nearly doubled from October (15 mm) to December (28 mm), despite having 25 percent less median *P* (82 mm in October, 60 mm in December) (table 4). Further analysis of a longer period of record is needed to determine if a late-year increase in *ETa* is an annual pattern or a result of specific climatic conditions in 2015.

Monthly available water (fig. 6*C*) was at a minimum in August (median = −49.3 mm) and at a maximum in October (median = 68.0 mm). Median available water typically was less during the growing season (April–September, mean = −17 mm) than outside of the growing season (mean = 28 mm). This pattern was generally opposite that of *ETa* (fig. 6*A*). Within the growing season, only May (median *P* – *ETa* = 3 mm) and July (median *P* – *ETa* = 24 mm) had enough precipitation to increase available water levels in the East Mountain area. The maximum available water in October (fig. 6*C*) resulted from relatively large *P* compared to *ETa*; during one late-October event, the Sandia Middle station recorded 38 mm of *P* (10 mm on October 20 and 28 mm on October 21), and the Tijeras station recorded 27 mm of *P* (6 mm on October 20 and 21 mm on October 21), which was about one-half of the monthly *P* for each station. At a time when most plants have minimal transpiration, this large precipitation event directly translated into surplus available water. This available water likely contributed to surface runoff and groundwater recharge, and increased soil moisture, which in turn contributed to increased *ETa* in November and December.

Spatial and Temporal Variability of *ETa* and Available Water

Annual *ETa* (fig. 7*A*) generally followed a similar spatial pattern to that of land cover (fig. 4). Greater *ETa* was observed in areas of evergreen forest, and lesser *ETa* was observed in areas of deciduous forest, mixed forest, shrub, and herbaceous land cover. The spatial pattern of annual available water (*P* – *ETa*, fig. 7*C*) generally was reversed from *ETa*. Greater available water was observed in areas of deciduous forest, mixed forest, shrub, and herbaceous land cover and lesser available water in areas of evergreen forest. This pattern was somewhat mediated by the spatial pattern of annual total *P* (fig. 7*B*), which was greater in the higher-elevation northwestern region near the crest of the Sandia Mountains and in the higher-elevation southwestern region of the Manzanita Mountains.

Monthly *ETa* (fig. 8) retained some of the spatial patterns evident in annual *ETa* (fig. 7*A*) overlaid on a large seasonal variation. *ETa* magnitude generally was greatest in July and smallest in January, but the transition months did not show smooth temporal or consistent spatial changes from month to month. For example, although *ETa* in some areas increased from February to March, *ETa* in other areas decreased over that same period. Similarly, from May to June, areas of increasing and decreasing *ETa* were both observed. Temporal and spatial variability in *ETa* may both relate to interactions of vegetation phenology, soil moisture, and timing of *P* and other climatic variables such as air temperature, cloud cover, and wind speed. For example, a large increase in *ETa* was observed from April to May (fig. 8), corresponding to higher *P* over much of the East Mountain area in May (fig. 9).

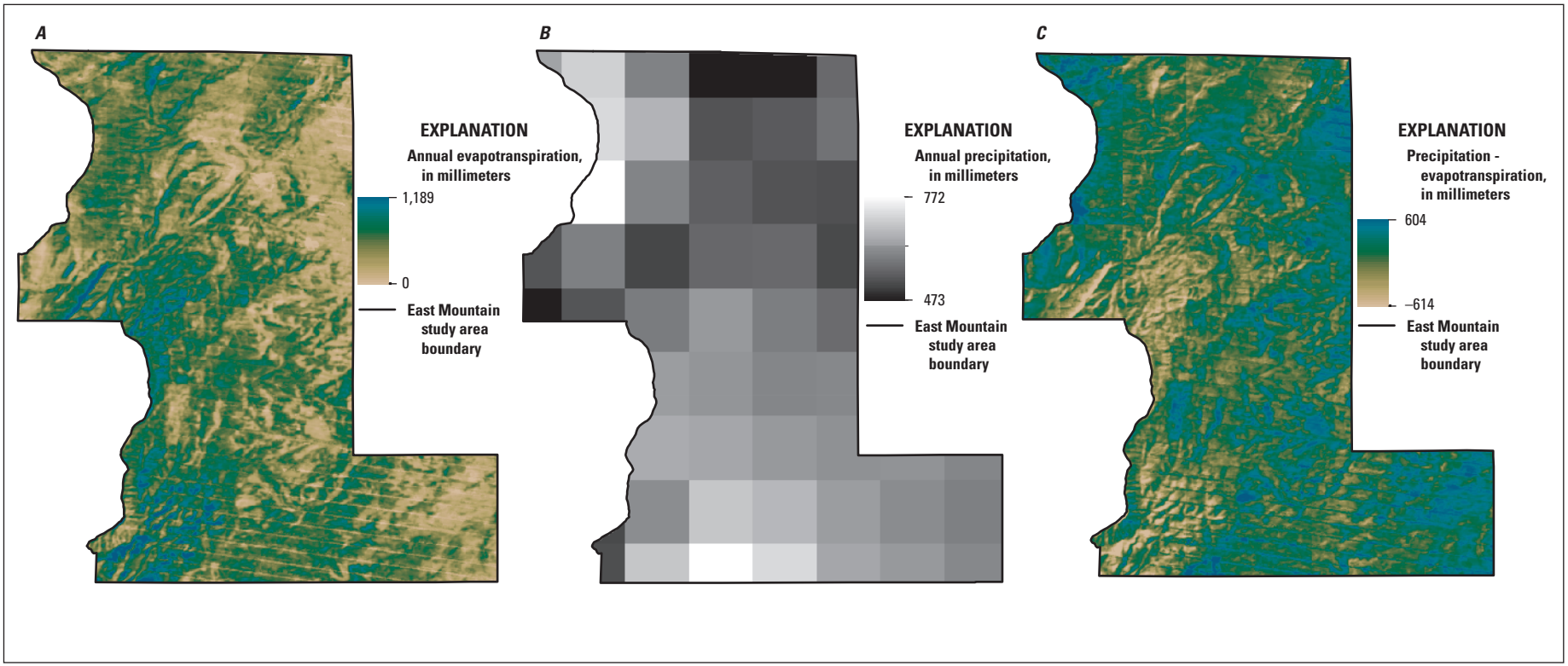

Figure 7. *A*, Annual actual evapotranspiration (*ETa*), *B*, precipitation (*P*), and *C*, available water (*P* – *ETa*) in the East Mountain area of Bernalillo County, New Mexico, 2015.

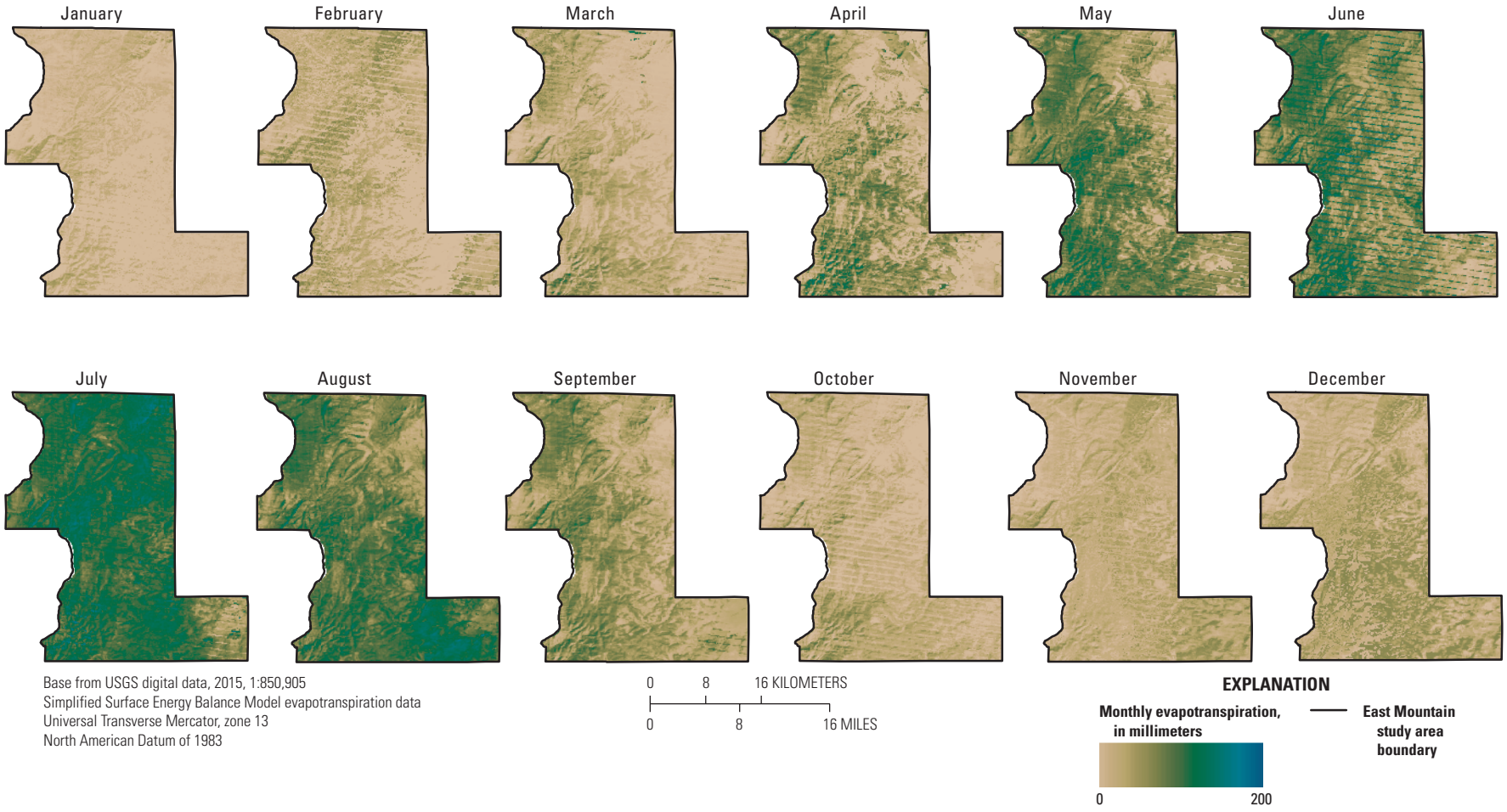

Figure 8. Monthly actual evapotranspiration (*ETa*) in the East Mountain area of Bernalillo County, New Mexico, 2015.

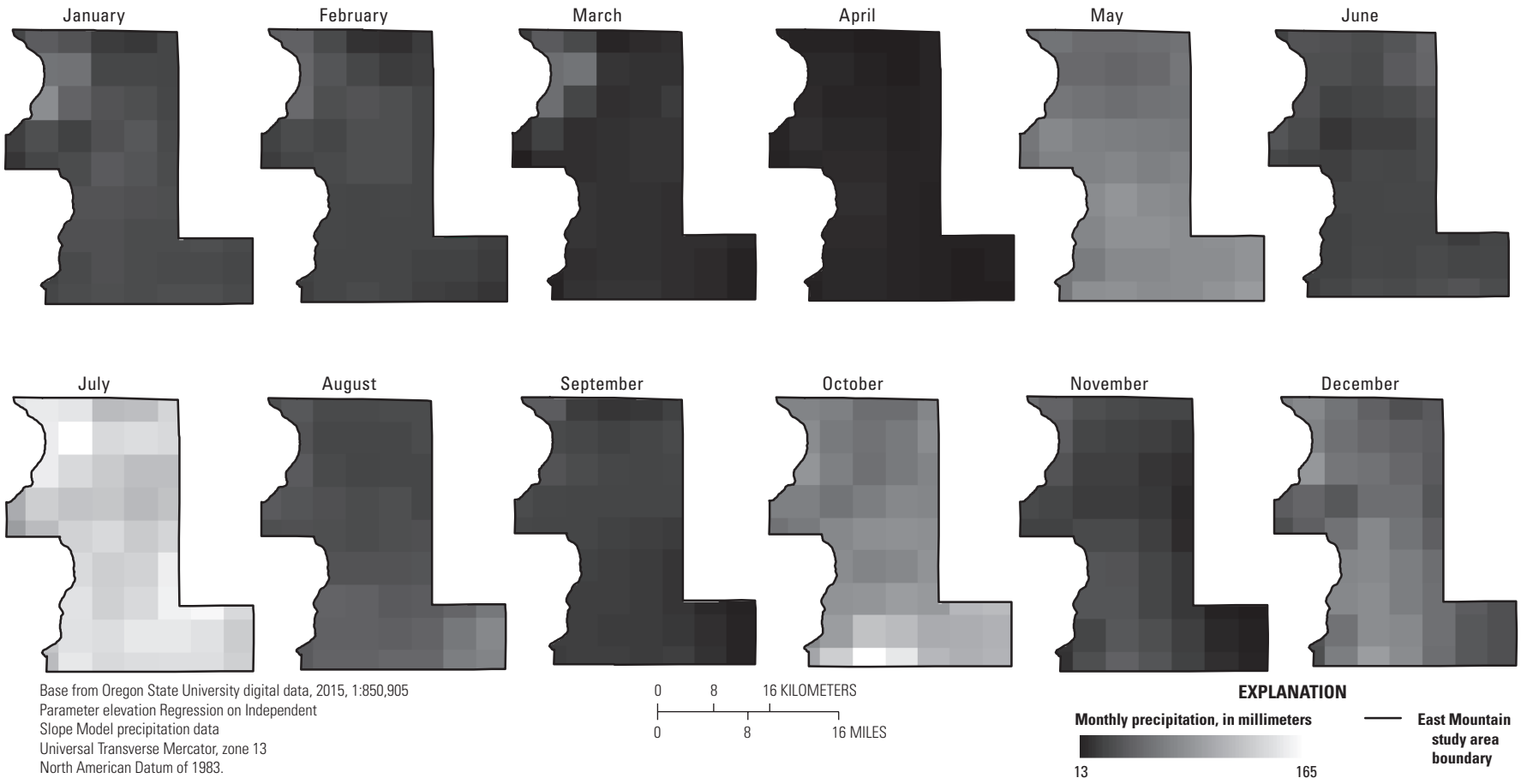

Figure 9. Monthly precipitation (*P*) in the East Mountain area of Bernalillo County, New Mexico, 2015.

Monthly available water (fig. 10) combines the effects of *P* and *ETa* on a monthly basis and provides insights into their interactions. Months with lower *ETa* (October–March, fig. 8) also tended to have greater available water (fig. 10), indicating that soil moisture and potential ET may have been largely out of phase. Spatial patterns in *ETa* from April through September generally reflected the spatial patterns of available water, with areas of lower *ETa* having greater available water and areas with greater *ETa* having lower available water (fig. 10). Localized areas of greater available water were also evident, particularly in May, July, and October (fig. 10). The locations of greater available water appeared to be driven by lower *ETa* (such as in the southeastern area during July, fig. 8), greater P (such as the southcentral area during October, fig. 9), or both.

Landscape and Climatic Effects on *ETa* and Available Water

Correlation analyses between annual *ETa* and each atmospheric, topographic, soil, and vegetation predictor variable yielded a p value $< 2.2 \times 10^{-16}$, indicating that the slope of each linear model differed significantly from zero ($p < 0.05$, table 7). Among nonatmospheric variables, the greatest R^2 was for TreeCanopy (0.46), followed by AwatSt100 (0.19), SoilBD1 (0.18), and Slope (0.17). This indicates that none of the nonatmospheric predictor variables alone adequately explained the variability in annual *ETa* across the 773,414 pixels in the study area. In the best case, TreeCanopy explained 46 percent of the variability in annual *ETa* around its mean. This result demonstrates the complexity of ET dynamics in general, as well as the heterogeneity of atmospheric, topographic, soil, and vegetation characteristics in the East Mountain area (see "Description of Study Area").

Variables having a relatively high positive correlation with annual *ETa* ($r > 0$, $R^2 > 0.05$) included each monthly *ETa* dataset ($R^2 = 0.15$ to 0.78), TreeCanopy (0.46), SoilBD1 (0.18), Slope (0.17), P12 (0.13), P11 (0.11), P4 (0.10), P2015 (0.08), LAI (0.07), and Elevation (0.06) (table 7). Variables having a relatively high negative correlation with annual *ETa* ($r < 0$, $R^2 > 0.05$) included AwatSt100 (0.19), Sand1 (0.13), SoilZMx (0.09), AwatSt025 (0.08), and Eastness (0.07). Variables having almost zero correlation with annual *ETa* ($R^2 \leq 0.01$) included Northness, Silt1, Clay1, Albedo, NDVI, P5, P8, and P9.

The parametric one-way ANOVA tests for categorical datasets (table 8) yielded p values $< 2.2 \times 10^{-16}$ for the variables LandcoverType and PartSize, indicating that annual mean *ETa* values differed significantly ($p < 0.05$) between two or more groups for both variables. Parametric multiple comparison tests were then performed to determine which variable groupings within each dataset (LandcoverType, PartSize) had different mean *ETa* values (table 9). An "association" between two groups, shown as two or more "X" entries in a column in table 9, indicates that those groups were not proven to be statistically different from one another, given a significance level (α) = 0.05 ($p > 0.05$). Analyses in this report will refer to LandcoverType group names listed in table 9.

For the variable LandcoverType, the evergreen forest land-cover group had the highest overall mean *ETa* value (613.8 mm), which was significantly greater ($p < 0.05$) than any other land-cover group (table 9). The second and third highest mean *ETa* values were within mixed forest (552.4 mm) and woody wetlands (530.0 mm) groups, which were statistically indifferentiable ($p > 0.05$) from each other, but statistically different ($p < 0.05$) than all other landcover groups. The fourth and fifth highest mean *ETa* values were within developed open (491.7 mm) and deciduous forest (460.2 mm) groups, which were each significantly different from each other and all other land-cover groups. Emergent herbaceous wetlands, developed low, and barren land groups were statistically indifferentiable from one another ($p > 0.05$) as were barren land, shrub (shrub/scrub), and developed medium groups. The lowest mean *ETa* values were within developed high and herbaceous groups, which had about one-half the *ETa* of the highest group (evergreen forest).

For the variable PartSize, mean *ETa* values from each group differed significantly from mean *ETa* values of every other group (table 9). The six PartSize groups (in order of decreasing mean *ETa*) were clayey-skeletal, loamy-skeletal, loamy, fine, fine-loamy, and fine-silty. The clayey-skeletal soil group had the highest mean *ETa* value at 621.8 mm, almost twice the mean *ETa* of the lowest group, fine-silty soils, at 308.3 mm.

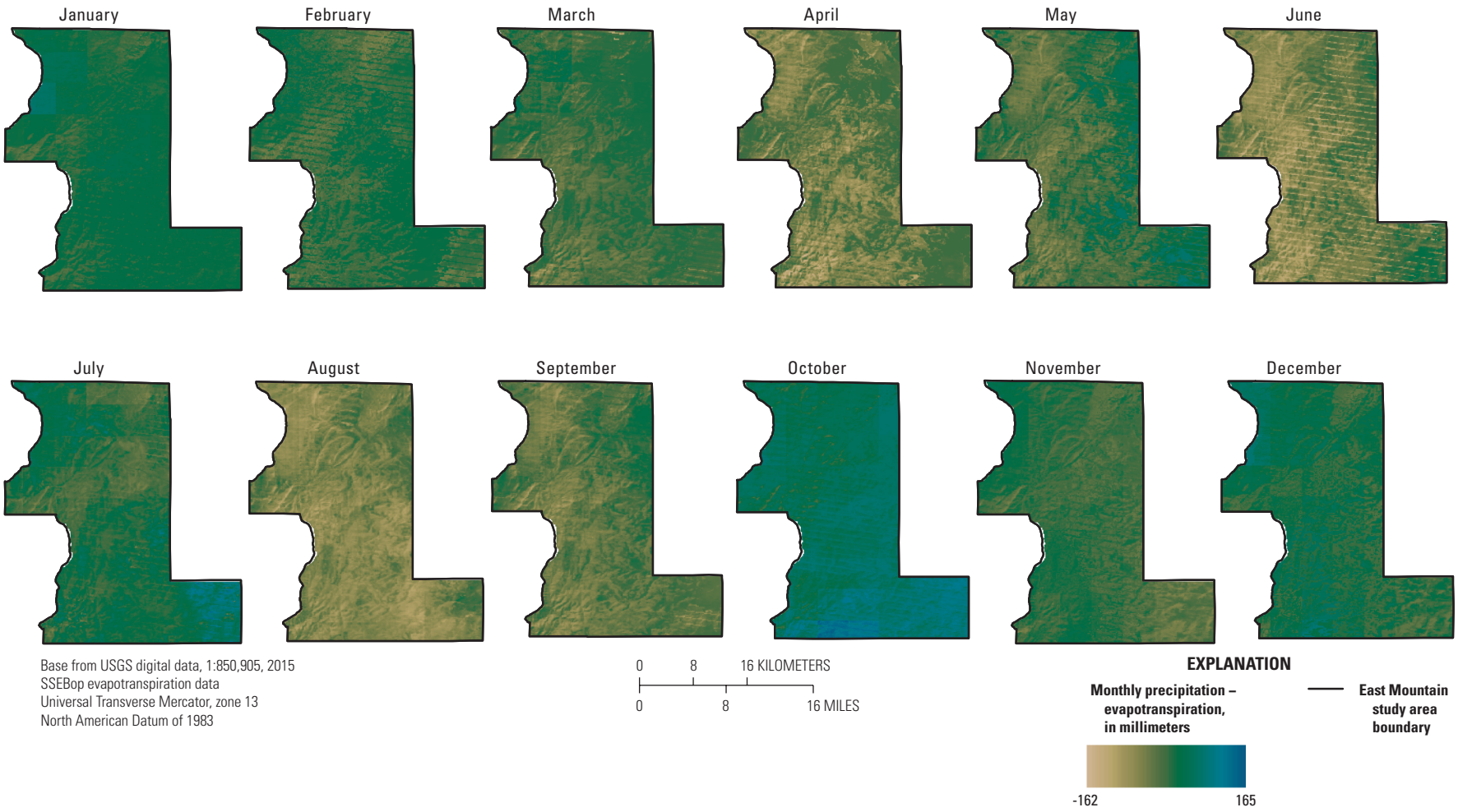

Figure 10. Maps showing monthly available water (precipitation minus actual evapotranspiration [*P* – *ETa*]) in the East Mountain area of Bernalillo County, New Mexico, 2015.

Table 7. Summary of annual actual evapotranspiration regression (*ETa*) analyses in the East Mountain area, Bernalillo County, New Mexico.

[Annual *ETa* is the dependent variable and other datasets are the independent variables. Refer to table 3 for dataset name abbreviations and more detailed information about each dataset. r, Pearson r; R^2, coefficient of determination; p, probability value; *b*, y intercept; *m*, slope; LAI, leaf area index; NDVI, Normalized Difference Vegetation Index]

Variable name, units	r	R^2	p	*b*	*m*
Actual evapotranspiration					
ETa1, millimeters	0.51	0.26	$<2.2 \times 10^{-16}$	473.69	9.23
ETa2, millimeters	0.38	0.15	$<2.2 \times 10^{-16}$	469.79	3.87
ETa3, millimeters	0.83	0.69	$<2.2 \times 10^{-16}$	383.41	7.87
ETa4, millimeters	0.83	0.69	$<2.2 \times 10^{-16}$	349.56	5.05
ETa5, millimeters	0.86	0.75	$<2.2 \times 10^{-16}$	186.28	5.31
ETa6, millimeters	0.76	0.58	$<2.2 \times 10^{-16}$	234.53	4.20
ETa7, millimeters	0.59	0.35	$<2.2 \times 10^{-16}$	29.94	4.71
ETa8, millimeters	0.70	0.49	$<2.2 \times 10^{-16}$	97.78	4.96
ETa9, millimeters	0.89	0.78	$<2.2 \times 10^{-16}$	229.45	6.79
ETa10, millimeters	0.79	0.62	$<2.2 \times 10^{-16}$	377.66	9.04
ETa11, millimeters	0.45	0.21	$<2.2 \times 10^{-16}$	404.49	5.91
ETa12, millimeters	0.39	0.15	$<2.2 \times 10^{-16}$	430.59	3.70
Precipitation					
P2015, millimeters	0.28	0.08	$<2.2 \times 10^{-16}$	60.22	0.80
P1, millimeters	0.18	0.03	$<2.2 \times 10^{-16}$	403.71	3.66
P2, millimeters	0.16	0.03	$<2.2 \times 10^{-16}$	379.00	4.96
P3, millimeters	0.15	0.02	$<2.2 \times 10^{-16}$	473.25	2.81
P4, millimeters	0.31	0.10	$<2.2 \times 10^{-16}$	87.92	27.03
P5, millimeters	0.09	0.01	$<2.2 \times 10^{-16}$	429.21	1.59
P6, millimeters	–0.22	0.05	$<2.2 \times 10^{-16}$	807.91	–7.88
P7, millimeters	0.20	0.04	$<2.2 \times 10^{-16}$	137.23	3.03
P8, millimeters	–0.03	0.00	$<2.2 \times 10^{-16}$	564.71	–0.50
P9, millimeters	0.11	0.01	$<2.2 \times 10^{-16}$	425.53	4.06
P10, millimeters	0.13	0.02	$<2.2 \times 10^{-16}$	447.68	1.09
P11, millimeters	0.33	0.11	$<2.2 \times 10^{-16}$	268.38	8.53
P12, millimeters	0.37	0.13	$<2.2 \times 10^{-16}$	254.60	4.80
Topography					
Elevation, meters	0.24	0.06	$<2.2 \times 10^{-16}$	–35.58	0.27
Slope, degrees	0.41	0.17	$<2.2 \times 10^{-16}$	446.82	4.23
Northness, fraction	0.12	0.01	$<2.2 \times 10^{-16}$	547.04	31.19
Eastness, fraction	–0.26	0.07	$<2.2 \times 10^{-16}$	561.05	–71.04

Table 7. Summary of annual actual evapotranspiration regression (*ETa*) analyses in the East Mountain area, Bernalillo County, New Mexico.—Continued

[Annual *ETa* is the dependent variable and other datasets are the independent variables. Refer to table 3 for dataset name abbreviations and more detailed information about each dataset. r, Pearson r; R^2, coefficient of determination; p, probability value; *b*, y intercept; *m*, slope; LAI, leaf area index; NDVI, Normalized Difference Vegetation Index]

Variable name, units	r	R^2	p	*b*	*m*
		Soil			
SoilZ1, centimeters	0.17	0.03	$<2.2 \times 10^{-16}$	519.18	0.06
Clay1, percent	–0.05	0.00	$<2.2 \times 10^{-16}$	562.55	–1.28
Silt1, percent	0.11	0.01	$<2.2 \times 10^{-16}$	508.38	1.26
Sand1, percent	–0.36	0.13	$<2.2 \times 10^{-16}$	664.69	–3.17
SoilK1, percent	–0.17	0.03	$<2.2 \times 10^{-16}$	601.49	–2.11
AWC1, fraction	–0.16	0.02	$<2.2 \times 10^{-16}$	–482.70	768.70
SoilBD1, percent	0.43	0.18	$<2.2 \times 10^{-16}$	602.70	–513.80
SoilZMx, centimeters	–0.31	0.09	$<2.2 \times 10^{-16}$	714.09	–16.46
AWatSt025, centimeters	–0.28	0.08	$<2.2 \times 10^{-16}$	709.89	–0.14
AWatSt100, centimeters	–0.44	0.19	$<2.2 \times 10^{-16}$	772.46	–65.14
		Vegetation			
TreeCanopy, percent	0.68	0.46	$<2.2 \times 10^{-16}$	299.02	8.26
LAI, percent	0.26	0.07	$<2.2 \times 10^{-16}$	447.36	4.96
NDVI, ratio	0.02	0.00	$<2.2 \times 10^{-16}$	539.92	28.69
Albedo, fraction	–0.03	0.00	$<2.2 \times 10^{-16}$	563.73	–97.48

Table 8. Summary of parametric multiple comparison tests for grouped annual actual evapotranspiration (*ETa*) datasets in the East Mountain area, Bernalillo County, New Mexico, 2015.

[Refer to table 3 for dataset variable names and more detailed information about each dataset. chi-squared, Pearson chi-squared statistic; df, degrees of freedom; p, probability value]

Variable name	Chi-squared	df	p
LandcoverType	296,890	11	$<2.2 \times 10^{-16}$
PartSize	122,250	6	$<2.2 \times 10^{-16}$

Table 9. Summary of parametric multiple comparison tests for the LandcoverType and PartSize (soil texture) datasets in the East Mountain area, Bernalillo County, New Mexico, 2015.

Group name	Annual mean *ETa* (millimeters)	Size (number of pixels)	Groups of statistical association at $\alpha = 0.05$[1]						
		LandcoverType							
Evergreen forest	613.8	535,950	X						
Mixed forest	552.4	2,147		X					
Woody wetlands	530.0	203		X					
Developed open	491.7	29,789			X				
Deciduous forest	460.2	5,307				X			
Emergent herbaceous wetlands	436.6	510					X		
Developed low	426.3	4,572					X		
Barren land	409.9	123					X	X	
Shrub	389.3	93,913						X	
Developed medium	387.9	581						X	
Developed high	321.3	100							X
Herbaceous	308.5	87,901							X
		PartSize							
Clayey-skeletal	621.8	36,072	X						
Loamy-skeletal	609.7	151,290		X					
Loamy	594.1	120,379			X				
Fine	455.8	285,918				X			
Fine-loamy	431.0	25,092					X		
Fine-silty	308.3	36						X	

[1] *ETa* values for LandcoverType groups and PartSize groups that have X entries in the same column are not statistically different at an alpha (α) value of 0.05.

Regression Analyses

Results of regression analyses are presented in this section. Regression analyses were done between monthly *ETa* and annual *ETa*, precipitation and *ETa*, topographic variables and *ETa*, vegetation variables and *Eta*, and soil variables and *ETa*.

Monthly *ETa* and Annual *ETa*

Monthly *ETa* for some months in the growing season had the highest correlations to annual *ETa* among the tested variables (table 7). For each regression analysis, R^2 values indicate the degree of correlation between the spatial pattern of the test variable and the spatial pattern of annual *ETa*. Each monthly *ETa* dataset had a positive r value, indicating a positive relation (> 0.15) with annual *ETa*. Specifically, and in this order, September (ETa9), May (ETa5), April (ETa4), March (ETa3), October (ETa10), June (ETa6), and August (ETa8) had the highest correlations (R^2 ranging from 0.49 to 0.78). Compared to *ETa* during months in the middle part of the growing season (June, July, and August [ETa6 to ETa8]), *ETa* during months in both the early (March, April, and May [ETa3 to ETa5]) and late portions of the growing season (September [ETa9]) were better predictors of annual *ETa*.

Precipitation and *ETa*

PRISM *P* datasets having the highest positive correlations with annual *ETa* were P12 ($R^2 = 0.13$), P11 (0.11), P4 (0.10), and P2015 (0.08); all other months had $R^2 \leq 0.05$ (table 7). Annual *P* (P2015) and annual *ETa* had higher correlation ($R^2 = 0.08$, $m = 0.80$) than most monthly *P* datasets. If one assumes that all ET in 2015 was derived from precipitation that occurred during 2015, this result indicates that *ETa* was 80 percent of *P*, comparable to the 89 percent calculated as the ratio of mean *ETa* to mean *P* (table 4). Monthly *P* during the monsoon season (July to September) had lower correlations with annual *ETa*.

Topographic Variables and *ETa*

The topographic variables that had the highest correlations with annual *ETa* were Slope ($R^2 = 0.17$), Eastness (0.07), and Elevation (0.06) (table 7). Slope and Elevation had a positive correlation with annual *ETa*, whereas Eastness

had a negative correlation. Slope and Elevation tended to be better predictors of monthly *ETa* in spring and fall than during other seasons, with a midsummer decrease in correlation and minimum correlations in winter (table 10). Eastness correlations were more consistent among months (r between −0.17 and −0.26 for all but 3 months), with highest negative correlations in January and July. The negative correlation of Eastness reflected that cells having an easterly orientation were increasingly shaded in the afternoon, which reduced ET in those cells. Slope had the fourth highest correlation of all tested variables other than monthly *ETa* datasets. Several factors might have affected the correlation of Slope with *ETa*. For example, slopes probably were greatest in areas of high elevation (fig. 2), high *P* (fig. 9), and high tree density (fig. 5).

Vegetation Variables and *ETa*

The vegetation variables with the highest correlations with annual *ETa* were TreeCanopy ($R^2 = 0.46$) and, to a lesser extent, LAI ($R^2 = 0.07$) (table 7). TreeCanopy and LAI both had positive correlations with annual *ETa*, indicating that greater canopy densities typically yielded greater annual *ETa*. Additionally, among the 12 categorical LandcoverType groups present in the East Mountain area, there were 7 significantly different *ETa* levels (table 9), which reinforced the importance of vegetation on *ETa*. NDVI had minimal correlation with annual *ETa* (table 7) or monthly *ETa* (table 10).

TreeCanopy outperformed both LAI and NDVI as a predictor variable for annual *ETa*. This was a notable result because NDVI is generally found or assumed to correlate well with ET (Glenn and others, 2008; Haynes and Senay, 2012; DeJonge and others, 2016) because of the clear importance of vegetation density on ET. For a given vegetation density, however, the influences of net radiative energy and soil water limitation may also affect the actual ET. For example, Fisher and others (2008) found error in ET simulation to be highly sensitive to net radiation and moderately sensitive to NDVI. In this study, we found that TreeCanopy had higher correlation with *ETa* than either LAI or NDVI and hypothesize that this was because the spectral bands used to estimate tree canopy percentage included all seven ETM+ bands, including the thermal band, whereas NDVI (red, near-infrared) and LAI (red, near-infrared, short-wave-infrared) did not include the thermal band. This allowed TreeCanopy to better account for nonvegetation-related variability in *ETa*, such as net-energy limitation or water limitation, that may have occurred over the spatial and temporal domain of this study. Spatial scale did not appear to be a primary cause for this result, because *ETa* (100-m resolution data) had higher correlation with TreeCanopy (30 m, higher resolution) than with either NDVI (30 m, higher resolution) or LAI (300 m, lower resolution). Further assessment using data from multiple years and locations is needed to test this hypothesis.

Soil Variables and *ETa*

Several soil variables had higher correlations with annual *ETa* relative to other landscape variables. TreeCanopy was the only tested nonatmospheric variable that had a higher correlation than AwatSt100 ($R^2 = 0.19$) and SoilBD1 ($R^2 = 0.18$) (table 7). Other soil-related variables with notable correlations included Sand1 ($R^2 = 0.13$), SoilZMx ($R^2 = 0.09$), and AwatSt025 ($R^2 = 0.08$). Among these soil-related variables, only SoilBD1 had a positive correlation with annual *ETa*. The categorical soil variable PartSize was also an effective predictor of *ETa* (table 8), as the mean *ETa* of every soil particle size group differed from the mean *ETa* of every other particle size group (table 9).

Key Patterns in *ETa* and Available Water

Key patterns for *ETa* and available water are described in this section based on analyses of elevation, tree canopy, and soil texture.

Elevation

The annual *ETa* and *P* – *ETa* of each LandcoverType category were grouped by four elevation bands (fig. 11). Elevation patterns were analyzed because the Elevation variable had a relatively high correlation with annual *ETa* (table 7) and often influences changes in climate, vegetation, and soil type. Elevation bands were defined to coincide with distinct ecological zones (Julyan and Stuever, 2005). The lowest elevation band (1,752–2,000 m above NAVD 88) was dominated by juniper, black grama grass, and Chihuahuan Desert ecoregion plants such as oreganillo, mariola, and desert marigold. The low-mid elevation band (2,001–2,400 m above NAVD 88) ranged from juniper, pinon, and evergreen oak at lower elevations, to ponderosa pine and deciduous oaks at higher elevations. The high-mid elevation band (2,401–2,800 m above NAVD 88) consisted of a mixture of conifers and gambel oak. Finally, the high elevation band (2,801–3,254 m above NAVD 88) was dominated primarily by spruce and fir.

Among LandcoverType categories, annual median *ETa* was greatest for the evergreen, followed by mixed forest, developed open, deciduous, developed low, shrub, developed medium, developed high, and herbaceous (fig. 11*A*). Elevation explained some of the variability of *ETa* within natural (evergreen, mixed forest, deciduous forest, shrub, and herbaceous) and developed open areas, as each of these LandcoverType categories generally had increasing median *ETa* from the low to high-mid elevation bands, and decreasing median *ETa* from the high-mid to high elevation bands. The only exception was that shrub *ETa* decreased slightly between the low and low-mid elevation bands.

Table 10. Summary of annual and monthly actual evapotranspiration (*ETa*) Pearson-r values in the East Mountain area, Bernalillo County, New Mexico, 2015.

[*ETa* is the dependent variable and other datasets are the independent variables. Refer to table 3 for dataset variable names and more detailed information about each dataset. cm, centimeter; LAI, leaf area index; NDVI, Normalized Difference Vegetation Index]

Dataset, units	ETa2015	ETa1	ETa2	ETa3	ETa4	ETa5	ETa6	ETa7	ETa8	ETa9	ETa10	ETa11	ETa12
Topography													
Elevation, meters	0.24	−0.14	−0.08	0.32	0.39	0.22	0.26	0.08	0.22	0.31	0.20	−0.22	−0.06
Slope, degrees	0.41	0.28	0.20	0.40	0.37	0.43	0.47	0.26	0.12	0.50	0.26	−0.14	−0.11
Northness, fraction	0.12	0.20	0.15	0.11	0.04	0.04	0.05	0.11	0.07	0.09	0.09	0.14	0.05
Eastness, fraction	−0.26	−0.30	−0.21	−0.19	−0.17	−0.20	−0.21	−0.26	−0.05	−0.20	−0.18	−0.18	−0.11
Soil													
SoilZ1, cm	0.17	0.25	0.17	0.14	0.10	0.16	0.21	0.18	−0.05	0.16	0.15	0.00	−0.04
Clay1, percent	−0.05	−0.20	−0.11	−0.02	0.01	−0.03	−0.09	−0.12	−0.08	−0.02	−0.07	−0.05	0.04
Silt1, percent	0.11	−0.16	−0.06	0.09	0.15	0.11	0.03	0.00	0.18	0.10	0.07	0.03	0.14
Sand1, percent	−0.36	−0.26	−0.22	−0.31	−0.29	−0.35	−0.37	−0.28	−0.07	−0.36	−0.29	0.01	−0.01
SoilK1, percent	−0.17	−0.18	−0.13	−0.14	−0.12	−0.15	−0.19	−0.19	−0.01	−0.16	−0.15	0.01	−0.03
AWC1, fraction	−0.16	0.24	0.18	0.17	0.12	0.18	0.24	0.15	0.10	0.22	0.08	0.13	0.15
SoilBD1, percent	0.43	0.25	0.17	0.32	0.37	0.42	0.42	0.32	0.15	0.47	0.19	0.02	0.05
SoilZMx, cm	−0.31	0.03	0.00	−0.19	−0.29	−0.29	−0.20	−0.20	−0.28	−0.23	−0.22	−0.18	−0.27
AWatSt025, cm	−0.28	−0.24	−0.18	−0.27	−0.23	−0.32	−0.34	−0.20	−0.02	−0.38	−0.08	0.12	0.10
AWatSt100, cm	−0.44	−0.26	−0.19	−0.34	−0.37	−0.42	−0.42	−0.35	−0.16	−0.42	−0.29	−0.08	−0.10
Vegetation													
TreeCanopy, percent	0.68	0.14	0.14	0.59	0.68	0.65	0.56	0.37	0.46	0.68	0.51	0.07	0.20
LAI, percent	0.26	−0.03	−0.03	0.30	0.36	0.32	0.30	0.10	0.13	0.35	0.20	−0.29	−0.06
NDVI, ratio	0.02	0.02	0.04	0.03	0.03	−0.01	0.02	0.03	0.00	0.01	−0.01	0.01	0.00
Albedo, fraction	−0.03	0.08	0.09	0.10	0.09	0.02	0.01	0.10	0.14	0.01	0.19	0.01	0.00

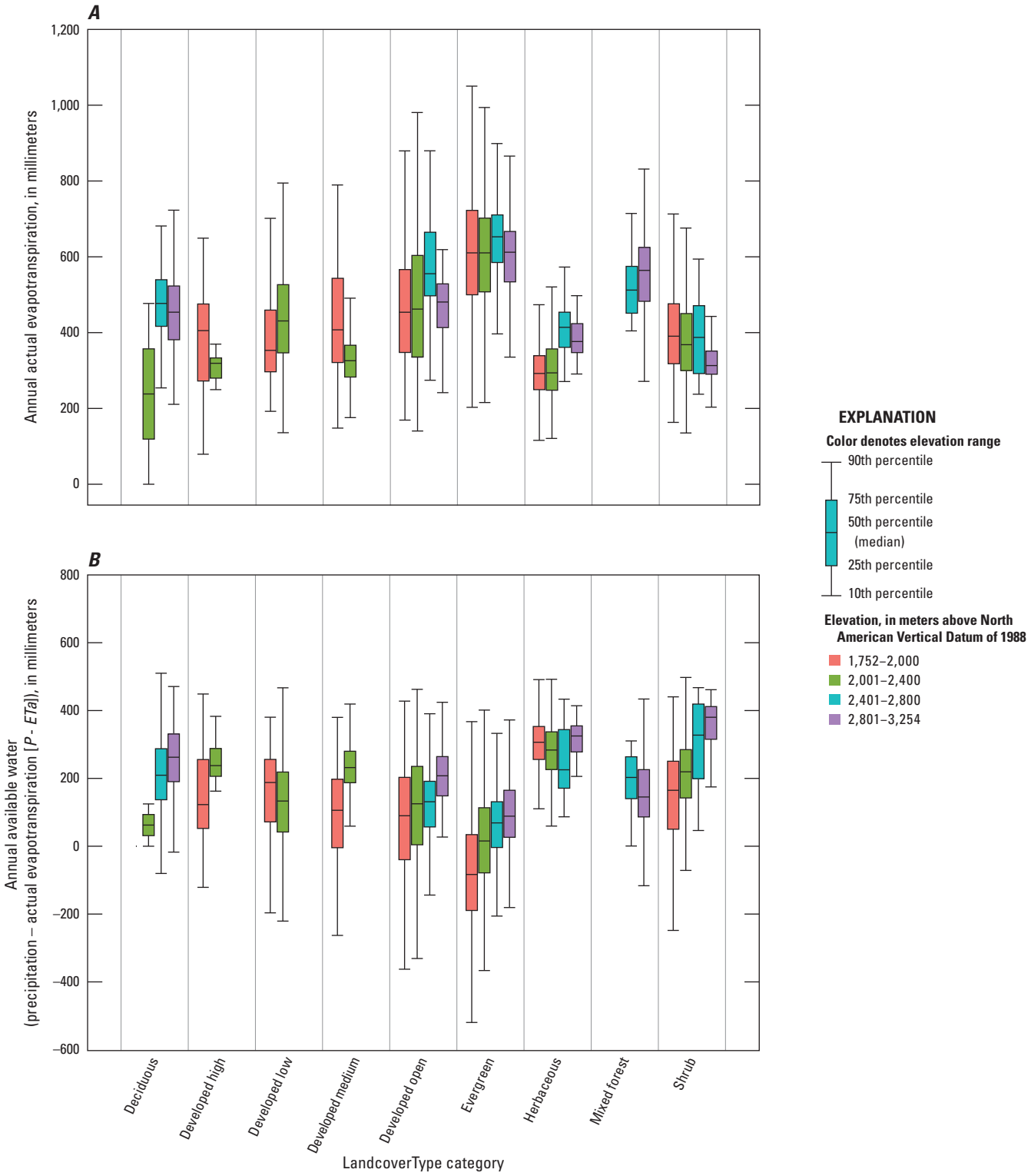

Figure 11. Effects of LandcoverType and Elevation on *A*, annual actual evapotranspiration (*ETa*) and, *B*, available water (*P* – *ETa*) of the primary landcover types for four elevation bands in the East Mountain area of Bernalillo County, New Mexico, 2015.

Elevation explained some of the variability of *P – ETa* within natural and developed open LandcoverType categories, and as such, *P – ETa* values (fig. 11*B*) were not simply inversely related to *ETa* (fig. 11*A*). The evergreen, deciduous, shrub, and developed open groups all had increasing median *P – ETa* with increasing Elevation values. This indicates that *P* increased more than *ETa* with increasing Elevation values, resulting in more available water at higher elevations. Herbaceous median *P – ETa* also was greatest for the highest elevation band, but *P – ETa* decreased from the low to high-mid elevation bands and then increased to a peak in the high elevation band. In contrast, median *P – ETa* for the mixed forest category decreased from the high-mid to high elevation bands. These results could potentially be caused by variations in grass, herb, and mixed forest density between elevation bands and (or) differing compositions of grasses, herbs, and trees in each elevation band. However, the large variability of *ETa* and *P – ETa* within each elevation band indicates that other factors in addition to elevation influence ET and available water in the East Mountain area.

Tree Canopy

TreeCanopy was analyzed as a group because this variable had the highest correlation with annual *ETa* of any tested variable other than monthly *ETa* datasets (table 7). Four TreeCanopy bands were defined using descriptive statistics. Tree canopy 0–18 percent spanned from the minimum to Q1, 19–30 percent from Q1 to the median, 31–42 percent from the median to Q3, and 43–72 percent from Q3 to the maximum. Annual median *ETa* within each LandcoverType category increased with increasing TreeCanopy cover (fig. 12*A*). The highest *ETa* was found in high density (43- to 72-percent tree canopy cover) evergreen forest and developed open areas. The greatest variability between annual median *ETa* among TreeCanopy levels within a LandcoverType category was for evergreen forest and developed open groups.

The relation between annual *ETa* and elevation indicated a general decrease in *ETa* from the high-mid to high elevation bands (fig. 11*A*), whereas the relation between *ETa* and TreeCanopy showed a consistent increase in *ETa* with increased TreeCanopy cover (fig. 12*A*). This indicates that decreased *ETa* between the high-mid and high elevation bands may be caused by a decrease in TreeCanopy cover in the highest elevation band. The high correlation between TreeCanopy and *ETa*, as well as the higher *ETa* values for LandcoverType categories dominated by trees, indicates that, overall, trees had a large effect on transpiration relative to other vegetation types in the area.

Annual median available water decreased in each LandcoverType category with increasing TreeCanopy cover (fig. 12*B*). The highest available water was found in low density areas having 0- to 18-percent tree canopy cover (mixed forest, deciduous, herbaceous, developed open and shrub groups), whereas the lowest available water was found in higher density evergreen and developed areas (developed low, developed medium, and developed high groups). These results are indicative of areas where greater *P* occurred. For example, given the relation between TreeCanopy and *ETa*, one would expect developed areas to have more available water and deciduous forest group to have less available water; however, *ETa* was offset by *P* in these areas (figs. 4, 7*B*).

Soil Texture

Soil texture (PartSize) was chosen as a group because it was the only analyzed categorical variable for which each group differed significantly from the others (table 9). Soil characteristics strongly influence storage and transmission of water through the East Mountain area, and thus affect the partitioning of P into water available for runoff, soil storage, ET, or groundwater recharge. This was demonstrated by the continuous variables AwatSt100 and SoilBD1 having among the highest correlations with annual *ETa* of any tested landscape variable (table 7).

Soil texture (PartSize) explained some of the variability in *ETa* within each LandcoverType category (fig. 13*A*). Overall, clayey-skeletal, loamy, and loamy-skeletal soils often had the highest *ETa* values within a given category, and fine, fine-loamy, and fine-silty soils often had the lowest *ETa* values, although fine-silty soil was rare. However, this pattern may have been driven by the vegetation density of evergreen forest and herbaceous LandcoverType categories within the study area (fig. 4), as the relations between soil texture and annual *ETa* differed notably between LandcoverType categories. Clayey-skeletal, loamy, and loamy-skeletal soils had the greatest *ETa* in herbaceous, evergreen, and developed open LandcoverType categories (fig. 13*A*). These soil types also were the only soil types that hosted the mixed forest group. In developed open LandcoverType areas, loamy and loamy-skeletal soil had greater *ETa* values than those for clayey-skeletal soil. In deciduous forest areas, fine soil had the highest *ETa*. In shrub areas, loamy and fine-loamy soils had the highest *ETa*.

The highest overall median *ETa* values were present in evergreen LandcoverType areas with clayey-skeletal and loamy-skeletal soil types, whereas fine-loamy soils had lesser median *ETa* values (fig. 13*A*). Clayey-skeletal and loamy-skeletal soil types also had higher *ETa* values within herbaceous areas. With the exception of shrub, each natural LandcoverType category had increased *ETa* in soils of either a fine or skeletal nature. This result corresponds with the negative correlation between annual *ETa* and Sand1 (tables 7, 10), as no natural LandcoverType category (except shrub) had its highest *ETa* in loamy soil.

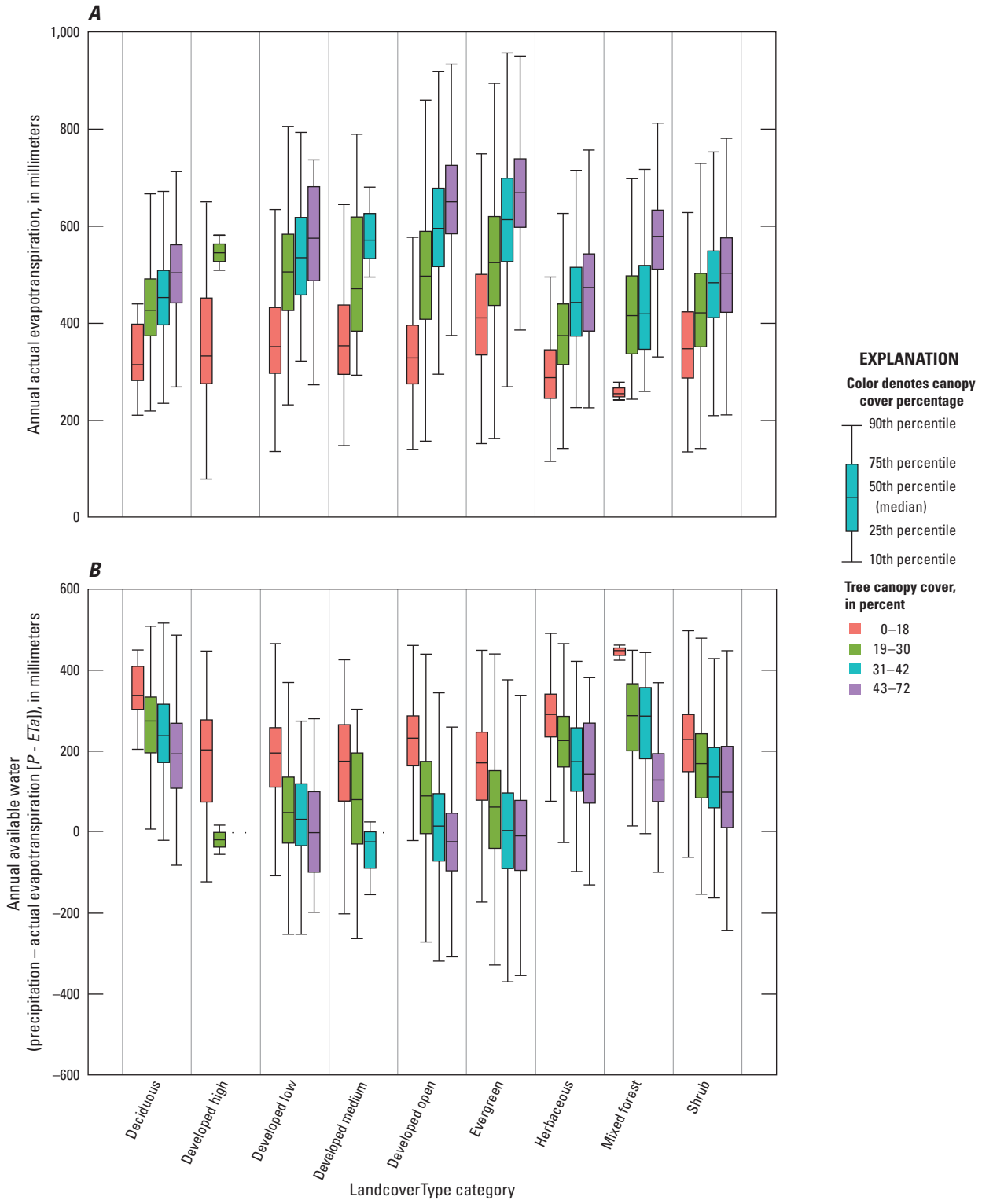

Figure 12. Effects of LandcoverType and TreeCanopy on *A*, annual actual evapotranspiration (*ETa*) and, *B*, available water (*P* – *ETa*) of the primary landcover types for four levels of tree-canopy cover in the East Mountain area of Bernalillo County, New Mexico, 2015.

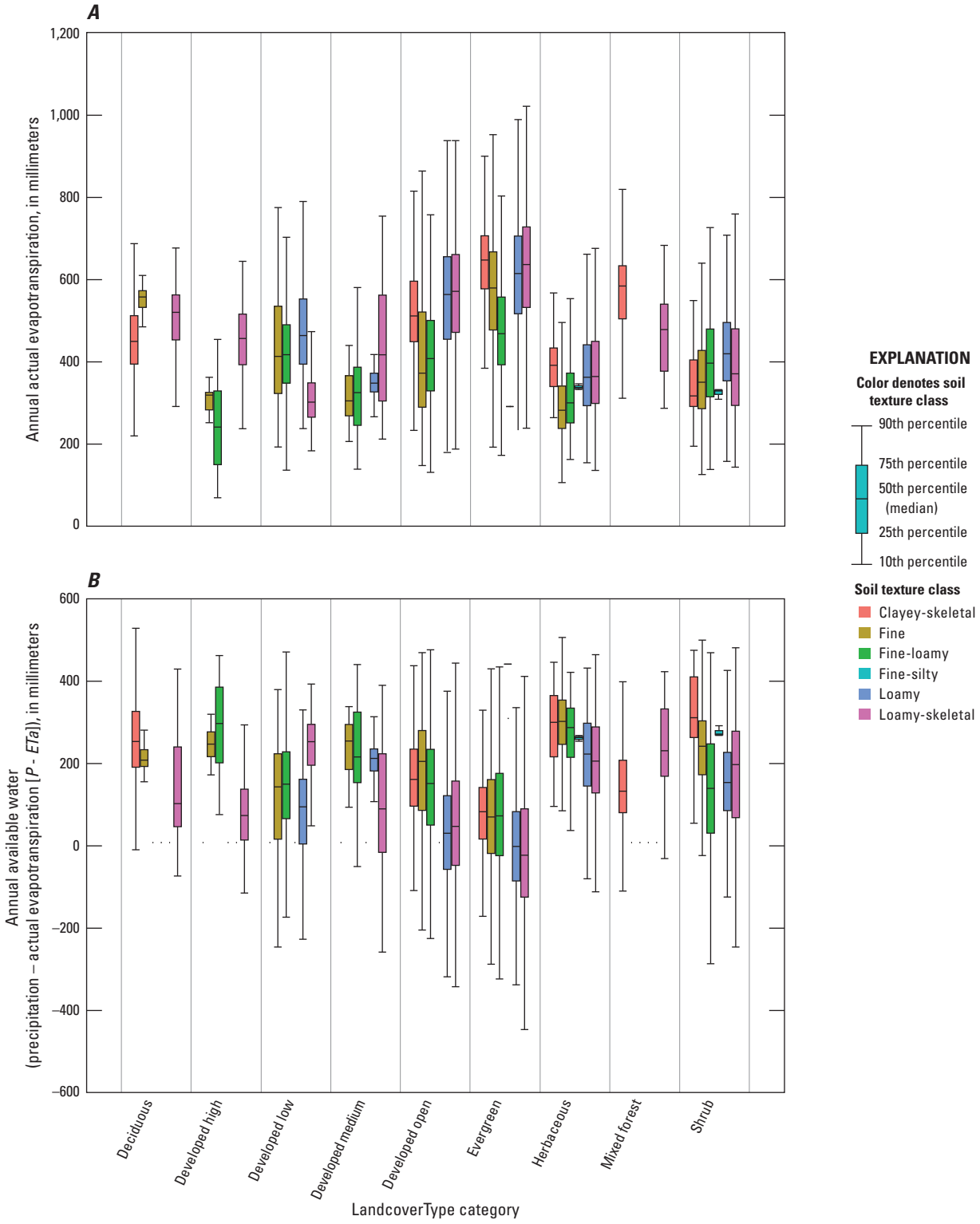

Figure 13. Effects of LandcoverType and soil texture (PartSize) on *A*, annual actual evapotranspiration (*ETa*) and, *B*, available water (*P* – *ETa*) of the primary landcover types for six soil texture classes in the East Mountain area of Bernalillo County, New Mexico, 2015.

Properties of soils related to soil texture and their interaction with *P – ETa* affect storage and transmittal of water through the soil and into the groundwater reservoir. In all natural landcover types (except the mixed forest group), finer soils (clayey-skeletal, fine, and fine-loamy) had the most available water, whereas coarser soils (loamy and loamy-skeletal) had the least available water. Relations of soil type with *P – ETa* were different than with *ETa*, indicating ET and available water have a complex response to differences in soil type. Further modeling would be useful in determining soils' infiltration, storage, conductivity, and plant-water availability relations to individual storms for each position in the landscape, as well as the corresponding effects of these processes on ET and available water.

A Multivariate Linear Model for East Mountain *ETa*

A summary of the multivariate model for annual *ETa* in the East Mountain is detailed in table 11. Monthly *ETa* models were created using the same methods and are summarized in table 12. Monthly *ETa* models include monthly *P* for all months in the year equal to or preceding the month being modelled (for example, January through July for the July *ETa* model).

The annual *ETa* and monthly *ETa* models each included nearly every parameter in the dataset. This was likely the result of having datasets with hundreds of thousands of values, in which case even variables with low correlation improved

Table 11. Summary of the best multivariate linear model for annual actual evapotranspiration (*ETa*) in the East Mountain area, Bernalillo County, New Mexico, 2015, as selected using the stepwise method.

[Refer to table 3 for variable name abbreviations. Residuals: minimum = −553.16, first quartile (Q1) = −69.53, median = −2.84, third quartile (Q3) = 69.14, maximum = 641.16. Residual standard error: 107.9 on 562,662 degrees of freedom (df); 210,734 missing observations were not used in analysis. Multiple coefficient of determination (R^2) = 0.6242; adjusted R^2 = 0.6242. F statistic: 5.192e+04 on 18 and 562,662 df. Probability value (p) <2.2×10^{-16}. Silt1 was excluded because of decreased model performance. t, t statistic; >, greater than; <, less than; NDVI, Normalized Difference Vegetation Index; LAI, leaf area index]

Model independent variable	Estimate	Standard error	t statistic	p
(Intercept)	713.5	9.688	73.6	<2.2×10^{-16}
Elevation	−0.2115	0.001362	−155.3	<2.2×10^{-16}
TreeCanopy	7.664	0.01525	502.4	<2.2×10^{-16}
SoilZMx	−0.02023	0.0009981	−20.3	<2.2×10^{-16}
Clay	3.539	0.2071	17.1	<2.2×10^{-16}
Slope	1.353	0.02413	56.1	<2.2×10^{-16}
SoilZ1	0.05866	0.003441	17.0	<2.2×10^{-16}
Albedo	−122.5	5.956	−20.6	<2.2×10^{-16}
AWatSt025	3.502	0.8301	4.2	0.000025
AWatSt100	−5.498	0.135	−40.7	<2.2×10^{-16}
Sand1	0.1703	0.04477	3.8	0.00014
SoilK1	−0.2438	0.02793	−8.7	<2.2×10^{-16}
AWC1	123.4	3.671	33.6	<2.2×10^{-16}
SoilBD1	−77.02	3.119	−24.7	<2.2×10^{-16}
NDVI	−1.852	1.217	−1.5	0.128
P2015	0.2923	0.003787	77.2	<2.2×10^{-16}
LAI	−1.592	0.01922	−82.8	<2.2×10^{-16}
Northness	28.63	0.2082	137.5	<2.2×10^{-16}
Eastness	−41.37	0.2255	−183.4	<2.2×10^{-16}

Table 12. Summary of the best multivariate linear models for annual and monthly actual evapotranspiration (*ETa*) in the East Mountain area, Bernalillo County, New Mexico, 2015, as selected using the stepwise method.

[Refer to table 3 for variable name abbreviations. R^2, coefficient of determination; df, degrees of freedom; F statistic, critical value; p, probability value; NA, not applicable]

Modeled variable	R^2	Standard error	df	F statistic	p	Excluded variables[1]
ETa2015	0.62	107.9	562,662	51,920	$<2.2 \times 10^{-16}$	Silt1
ETa1	0.27	7.79	564,467	10,900	$<2.2 \times 10^{-16}$	NA
ETa2	0.16	16.39	564,503	5,276	$<2.2 \times 10^{-16}$	NA
ETa3	0.50	13.06	565,132	26,030	$<2.2 \times 10^{-16}$	NA
ETa4	0.54	19.93	564,220	30,160	$<2.2 \times 10^{-16}$	NA
ETa5	0.59	19.16	565,395	33,740	$<2.2 \times 10^{-16}$	NA
ETa6	0.41	24.19	340,554	10,830	$<2.2 \times 10^{-16}$	Silt1, SoilZMx
ETa7	0.42	17.46	564,625	16,820	$<2.2 \times 10^{-16}$	Slope
ETa8	0.64	16.10	565,188	38,020	$<2.2 \times 10^{-16}$	NA
ETa9	0.65	13.95	564,347	40,110	$<2.2 \times 10^{-16}$	AWatSt100
ETa10	0.45	10.93	564,267	16,700	$<2.2 \times 10^{-16}$	NA
ETa11	0.33	10.48	343,851	6,369	$<2.2 \times 10^{-16}$	SoilK1, Silt1
ETa12	0.36	14.73	343,818	6,794	$<2.2 \times 10^{-16}$	P7, P6

[1]Excluded from the model using the stepwise selection algorithm.

overall model skill. As a result, variables were rarely excluded from *ETa* models. When they were, it appears to be the result of extensive cross-correlation with other variables during that timeframe. Differing R^2 values among the models show to what degree the monthly and annual models were able to account for variability in *ETa*.

The 2015 annual *ETa* (ETa2015) model had higher correlation ($R^2 = 0.62$) than all but two monthly *ETa* models, ETa8 and ETa9 (table 12). This result indicates that the chosen variables generally were better at predicting annual *ETa* than monthly *ETa*. This was likely due to an increase in variability in some variables on a monthly scale; for example, *P* was extremely variable month to month (fig. 9). The highest monthly correlations were during the growing season: $R^2 = 0.64$ for August (ETa8), $R^2 = 0.65$ for September (ETa9), and $R^2 > 0.40$ for each month from March (ETa3) through October (ETa10). This result indicates that these variables can most accurately model *ETa* when plants are actively transpiring and overall ET is highest. In particular, the monthly *ETa* models with the highest correlations (ETa8 and ETa9) followed a July having almost twice the mean precipitation (table 6). The resulting increase in soil moisture would have reduced limiting conditions for ET and appeared to allow higher correlations with the available combination of soil, vegetation, and topographic variables. The greater available moisture would also have provided conditions that better met the Penman-Monteith equation assumption of a wet evaporative surface. This result indicates that a soil-moisture variable is needed to more accurately model monthly *ETa*; however, an R^2 value of only 0.62 for the annual *ETa* model and a maximum of 0.65 for the best monthly *ETa* model indicates that more research is needed to better characterize the factors that govern *ETa* and *P* – *ETa* in the East Mountain area.

Summary and Conclusions

Evaporation from free-water surfaces and transpiration through plants, collectively known as evapotranspiration (ET), is a fundamental element of the water balance. Hydrologic systems partition precipitation (P) minus ET, referred to as available water, into soil water storage, streamflow, groundwater recharge, and ecosystem function. ET and available water vary spatiotemporally because of complex interactions between environmental factors, including vegetation characteristics, soil characteristics, topography, and climate. The U.S. Geological Survey, in cooperation with the Bernalillo County Public Works Division, conducted a 1-year study in 2015 to summarize ET and available water in the East Mountain area of New Mexico and analyze the potential effects of landscape and climatic factors on ET and available water.

Precipitation data from the Parameter-Elevation Regressions on Independent Slopes Model (PRISM) (*P*) were used in conjunction with actual ET (*ETa*) data from the Operational Simplified Surface Energy Balance (SSEBop) model to estimate available water (*P* – *ETa*) in the study area. Maps, descriptive statistics, regression analyses, and boxplots were used to characterize *P*, *ETa*, available water, topographic, soil, and vegetation data in the East Mountain area.

Supplementary boxplots were developed to further investigate some of the key landscape variables shown to relate to *ETa* and (or) available water. Five natural LandcoverType categories (evergreen, shrub, herbaceous, deciduous, and mixed forest) and four developed LandcoverType categories (developed open, developed low, developed medium, and developed high) were plotted. Variability within each LandcoverType category was further analyzed by using boxplots of annual *ETa* and *P* – *ETa* that subdivided each LandcoverType into Elevation, TreeCanopy, and PartSize (soil texture) categories.

Finally, linear multivariate models were developed for monthly and annual *ETa* as a function of landscape and *P* datasets selected using a stepwise algorithm (R script "step") with the Akaike information criterion. Monthly *ETa*, as well as *P* in months occurring after the modelled *ETa*, were excluded from the variable selection process, leaving the remaining monthly *P* datasets along with topography, vegetation, and soil characteristics as potential predictor variables.

Annual mean *P* in 2015 in the East Mountain area was 608 millimeters (mm), and annual mean *ETa* was 543 mm, indicating that in 2015 a spatial mean of about 65 mm of water was available for runoff, soil moisture replenishment, or groundwater recharge. However, *ETa* and *P* – *ETa* both varied substantially with time and location.

Monthly *ETa* retained some of the spatial patterns evident in annual *ETa*, though these patterns typically were most similar during the growing season. Although *ETa* was greatest in July and smallest in January, the intervening months did not show smooth temporal or consistent spatial changes from month to month. Perhaps limited water supply was a factor, as months with lower *ETa* (January to March, October to December) also tended to have greater available water, indicating that soil moisture and potential ET may have been largely out of phase.

Regression analyses showed that monthly *ETa* data had the highest coefficient of determination (R^2) values (up to 0.78) of any dataset regressed with annual *ETa*. Positive correlation typically was highest during the early and late parts of the growing season (March, April, May, and September). In contrast, monthly *P* was highly variable, and typically not highly correlated with annual *ETa*, as only November, December, and April had R^2 values greater than that of annual *P*. Annual *P* had an R^2 value of 0.08 and a slope of 0.80. If one assumes that all ET was from 2015 *P*, this result indicates that 80 percent of precipitation was *ETa*, comparable to the 89 percent calculated by the ratio of mean *ETa* to mean *P*.

The highest correlations with *ETa* among topographic variables were Slope ($R^2 = 0.17$), Eastness (0.07), and Elevation (0.06). Slope and Elevation each had a positive correlation with *ETa* and Eastness had a negative correlation. TreeCanopy ($R^2 = 0.46$) had the highest correlation of all vegetation characteristics, followed by leaf area index (LAI; $R^2 = 0.07$). Several soil characteristics correlated well with annual *ETa*. TreeCanopy was the only variable that had a higher correlation than AwatSt100 ($R^2 = 0.19$), SoilBD1 ($R^2 = 0.18$), and Sand1 ($R^2 = 0.13$). AwatSt100 and Sand1 had negative correlations with *ETa*, whereas SoilBD1 had a positive correlation.

ETa and *P* – *ETa* for nine major LandcoverType categories, including evergreen forest, mixed forest, deciduous forest, herbaceous, and shrub, as well as four levels of land development (developed open, developed low, developed medium, and developed high), were analyzed. Median *ETa* was highest for the evergreen forest category, followed by mixed forest, developed open, and deciduous forest. Herbaceous, shrub, and more developed LandcoverType categories each had a lower median *ETa*. Available water typically was highest for LandcoverType categories having the lowest *ETa*. Median available water was greatest for the herbaceous category, followed by deciduous forest, developed high, and shrub. Areas in the evergreen forest and mixed forest categories, as well as (other) less developed areas, had the lowest median available water. Areas in the deciduous forest category had the second highest median available water, despite having the fourth highest *ETa*. Areas in the deciduous forest category had greater *P* than most other areas.

The nine major LandcoverType categories were divided into four Elevation bands selected to represent distinct ecohydrological zones. *ETa* typically was greatest between elevations of 2,401 and 2,800 meters (m) above North American Vertical Datum of 1988 (NAVD 88), which is an area consisting primarily of conifers and gambel oak. The lower *ETa* at the highest elevations (2,801–3,254 m above NAVD 88) despite greater *P* may have been the result of decreased tree canopy cover or a shift from evergreen to deciduous trees with increased elevation, as deciduous forests had lower *ETa* on average.

Annual median *ETa* was shown to increase with TreeCanopy percentage, regardless of LandCoverType category. This pattern indicates that the presence of more trees or trees with larger canopies increased ET. TreeCanopy had higher correlation with *ETa* than did LAI or Normalized Difference Vegetation Index, which indicates that trees had a larger effect than other vegetation types on *ETa*. Given that tree canopy provides shade and is therefore unlikely to increase ground-surface evaporation, this result also indicates that *ETa* dynamics in the East Mountain area are highly influenced by transpiration rates. In contrast, available water was shown to increase with decreased TreeCanopy cover, indicating that areas with less tree canopy cover likely contributed more to runoff, soil moisture recharge, and (or) groundwater recharge.

Soil characteristics had higher correlation with annual *ETa* than did many other landscape characteristics. Grouping the nine major LandcoverType categories into six soil texture (PartSize) groups depicts relations of soil texture with annual *ETa* and *P – ETa*. Overall, loamy-skeletal and clayey-skeletal soil types had the greatest *ETa*. Loamy-skeletal and clayey-skeletal soils had the greatest *ETa* in the herbaceous and evergreen categories. These soil types also were the only soil types that hosted mixed forest. Areas in the developed open category had greater *ETa* in loamy soil than in clayey-skeletal soil. In the deciduous forest category, areas with fine soil had the highest *ETa*. In the shrub category, loamy and fine-loamy soils had the highest *ETa*. Differences in *ETa* among areas with similar soils were most likely influenced by unique root water-absorption techniques employed by different vegetation communities.

In all natural LandcoverType categories, finer soils (clayey-skeletal, fine, and fine-loamy) had the most available water, whereas coarser soils (loamy and loamy-skeletal) had the least available water. Fine-silty soil was rare in the study area. Relations of soil type with *P – ETa* were different than with *ETa*, indicating ET and available water have a complex response to differences in soil type. Further modeling would be useful in determining soils' infiltration, storage, conductivity, and plant-water availability relations to individual storms for each position in the landscape, as well as the corresponding effects of these processes on ET and available water.

The best multivariate linear model for annual *ETa* had an R^2 value of 0.62. Monthly *ETa* models had R^2 values between 0.16 and 0.65. Models usually, but not always, performed best during the growing season. These results indicate that even the best multivariate linear models cannot explain a notable amount of the variability in ET. The monthly *ETa* models with the highest correlations (August and September) followed a July with almost twice the mean precipitation, which would have reduced limiting conditions for ET, better met the Penman-Monteith equation assumption of a wet evaporative surface, and allowed higher correlations with a combination of soil, vegetation, and topographic variables. This result indicates that a soil-moisture variable is needed to more accurately model monthly *ETa*.

Two limitations of this study are noteworthy. First, the use of only a single year of data limited the breadth of combinations of available evaporative energy, available water, and vegetative conditions needed to develop a more meaningful correlative *ETa* model. A more robust, multiyear dataset would provide different combinations of environmental conditions for each growing season from which to develop a more robust multivariate model. Second, the use of readily available data sometimes forced spatial and temporal mismatches with the *ETa* dataset. Correlations almost certainly were reduced as a result of analysis of *ETa* at the 100-m spatial scale for a given year (2015) using temporally mismatched vegetation variables representing data collected in other years (such as 2011 for LandcoverType and TreeCanopy) or during specific times of the year (Normalized Difference Vegetation Index and existing vegetative cover from spring/summer) and using other variables at coarser spatial scales (such as 4-kilometer precipitation, 300-m LAI).

Further study is needed to better characterize this system, the variables that affect ET and available water, and the partitioning of available water into runoff, soil moisture storage, and groundwater recharge. Such a study could also span multiple years to capture a greater range of environmental variation and could seek to resolve the spatial-resolution mismatch of data sources. Continuing advances in the resolution and accuracy of satellite-derived geospatial data, including the key meteorological, vegetative, and soil moisture variables that influence ET, make it likely that future studies could include the additional variables (such as soil moisture) and higher resolutions (both spatially and temporally) needed to improve *ETa* model skill.

References Cited

Abatzoglou, J.T., 2013, Development of gridded surface meteorological data for ecological applications and modelling: International Journal of Climatology, v. 33, no. 1, p. 121–131. [Also available at https://doi.org/10.1002/joc.3413.]

Aho, K., Derryberry, D., and Peterson, T., 2014, Model selection for ecologists—The worldviews of AIC and BIC: Ecology, v. 95, p. 631–636. [Also available at https://doi.org/10.1890/13-1452.1.]

Akaike, H., 1974, A new look at the statistical model identification: IEEE Transactions on Automatic Control, v. 19, no. 6, p. 716–723. [Also available at https://doi.org/10.1109/TAC.1974.1100705.]

Alemayehu, T., van Griensven, A., Senay, G.B., and Bauwens, W., 2017, Evapotranspiration mapping in a heterogeneous landscape using remote sensing and global weather datasets—Application to the Mara Basin, East Africa: Remote Sensing, v. 9, no. 390, 24 p. [Also available at https://doi.org/10.3390/rs9040390.]

Allen, R.G., Pereira, L.S., Raes, D., and Smith, M., 1998, Crop evapotranspiration—Guidelines for computing crop water requirements: Rome, Italy, FAO Irrigation and Drainage Paper 56.

Allen, R.G., Tasumi, M., and Trezza, R., 2007, Satellite-based energy balance for mapping evapotranspiration with internalized calibration (METRIC)—Model: ASCE Journal of Irrigation and Drainage Engineering, v. 133, no. 4, p. 380–394.

Amatya, D.M., Irmak, S., Gowda, P., Sun, G., Nettles, J.E., and Douglas-Mankin, K.R., 2016, Ecosystem evapotranspiration—Challenges in measurements, estimates, and modeling: Transactions of the American Society of Agricultural and Biological Engineers, v. 59, no. 2, p. 555–560. [Also available at https://doi.org/10.13031/trans.59.11808.]

Arguez, A., Durre, I., Applequist, S., Vose, R.S., Squires, M.F., Yin, X., Heim, R.R., Jr., and Owen, T.W., 2012, NOAA's 1981–2010 U.S. climate normal—An overview: Bulletin of the American Meteorological Society, v. 93, p. 1687–1697. [Also available at https://doi.org/10.1175/BAMS-D-11-00197.1.]

Baret, F., Weiss, M., Lacaze, R., Camacho, F., Makhmara, H., Pacholcyzk, P., and Smets, B., 2013, GEOV1—LAI and FAPAR essential climate variables and FCOVER global time series capitalizing over existing products. Part 1—Principles of development and production: Remote Sensing of Environment, v. 137, p. 299–309. [Also available at https://doi.org/10.1016/j.rse.2012.12.027.]

Bastiaanssen, W.G.M., Menenti, M., Feddes, R.A., and Holtslag, A.A.M., 1998, The surface energy balance algorithm for land (SEBAL)—1. Formulation: Journal of Hydrology, v. 212–213, p. 198–212.

Chen, M., Senay, G.B., Singh, R.K., and Verdin, J.P., 2016, Uncertainty analysis of the Operational Simplified Surface Energy Balance (SSEBop) model at multiple flux tower sites: Journal of Hydrology, v. 536, p. 384–399. [Also available at https://doi.org/10.1016/j.jhydrol.2016.02.026.]

Copernicus Global Land Service, 2017, Leaf area index 300 m dataset: Accessed August 1, 2017, at http://land.copernicus.eu/global/products/lai.

Daly C., 2006. Guidelines for assessing the suitability of spatial climate data sets: International Journal of Climatology, v. 26, no. 6, p. 707–721.

Daly C., Halbleib M., Smith J.I., Gibson W.P., Doggett M.K., Taylor G.H., Curtis J., and Pasteris P.P., 2008, Physiographically sensitive mapping of climatological temperature and precipitation across the conterminous United States: International Journal of Climatology, v. 28, no. 15, p. 2031–2064.

Daly, C., Taylor, G., Gibson, W., Parzybok, T., Johnson, G., and Pasteris, P., 2000, High-quality spatial climate data sets for the United States and beyond: Transactions of the American Society of Agricultural and Engineers, v. 43, p. 1957–1962.

DeJonge, K.C., Mefford, B.S., and Chávez, J.L., 2016, Assessing corn water stress using spectral reflectance: International Journal of Remote Sensing, v. 37, no. 10, p. 2294–2312. [Also available at https://doi.org/10.1080/01431161.2016.1171929.]

Esri, 2017, ArcMap: Release 10.5.1: Redlands, California, Environmental Systems Research Institute.

Farr, T.G., and Kobrick, M., 2000, Shuttle radar topography mission produces a wealth of data: Eos, Transactions American Geophysical Union, v. 81, no. 48, p. 583–585.

Fisher, J.B., Tu, K., and Baldocchi, D.D., 2008, Global estimates of the land-atmosphere water flux based on monthly AVHRR and ISLSCP-II data, validated at 16 FLUXNET sites: Remote Sensing of Environment, v. 112, no. 3, p. 901–919.

Glenn, E.P., Huete, A.R., Nagler, P.L., and Nelson, S.G., 2008, Relationship between remotely-sensed vegetation indices, canopy attributes and plant physiological processes—What vegetation indices can and cannot tell us about the landscape: Sensors, v. 8, no. 4, p. 2136–2160. [Also available at https://doi.org/10.3390/s8042136.]

Gowda, P.H., Chavez, J.L., Colaizzi, P.D., Evett, S.R., Howell, T.A., and Tolk, J.A., 2007, Remote sensing based energy balance algorithms for mapping ET—Current status and future challenges: Transactions of the American Society of Agricultural and Biological Engineers, v. 50, no. 5, p. 1639–1644. [Also available at https://doi.org/10.13031/2013.23964.]

Hargreaves, G.H., and Samani, Z.A., 1985, Reference crop evapotranspiration from temperature: Applied Engineering in Agriculture, v. 1, no. 2, p. 96–99. [Also available at https://doi.org/10.13031/2013.26773.]

Haynes, J.V., and Senay, G.B., 2012, Evaluation of the relation between evapotranspiration and normalized difference vegetation index for downscaling the simplified surface energy balance model: U.S. Geological Survey Scientific Investigations Report 2012–5197, 8 p. [Also available at https://doi.org/10.3133/sir20125197.]

Helsel, D.R., and Hirsch, R.M., 2002, Statistical methods in water resources: U.S. Geological Survey Techniques of Water Resources Investigations, book 4, chap. A3, 522 p.

Homer, C.G., Dewitz, J.A., Yang, L., Jin, S., Danielson, P., Xian, G., Coulston, J., Herold, N.D., Wickham, J.D., and Megown, K., 2015, Completion of the 2011 national land cover database for the conterminous United States—Representing a decade of land cover change information: Photogrammetric Engineering and Remote Sensing, v. 81, p. 345–354.

Huang, C., Yang, L., Wylie, B.K., and Homer, C., 2001, A strategy for estimating tree canopy density using Landsat 7 ETM+ and high resolution images over large areas, *in* Proceedings of the Third International Conference on Geospatial Information in Agriculture and Forestry, Denver, Colorado, 5–7 November: Publications of the US Geological Survey 111. [Also available at http://digitalcommons.unl.edu/usgspubs/111.]

Irons, J.R., Dwyer, J.L., and Barsi, J.A., 2012, The next Landsat satellite—The Landsat data continuity mission: Remote Sensing of Environment, v. 122, p. 11–21.

Julyan, R., and Stuever, M., eds., 2005, Field guide to the Sandia Mountains: Albuquerque, N. Mex., University of New Mexico Press, 272 p.

Kottek, M., Grieser, J., Beck, C., Rudolf, B., and Rubel, F., 2006, World map of the Köppen-Geiger climate classification updated: Meteorologische Zeitschrift, v. 15, no. 3, p. 259–263. [Also available at https://doi.org/10.1127/0941-2948/2006/0130.]

Martin, D.L., and Gilley, J.R., 1993, Irrigation water requirements, chap. 2 *of* Part 623 National Engineering Handbook: Washington, D.C., Natural Resources Conservation Service, 284 p.

Monteith, J.L., 1965, Evaporation and environment, *in* Proceedings of the XIXth Symposium of the Society for Experimental Biology—The State and Movement of Water in Living Organisms: Cambridge, U.K., Cambridge University Press, p. 205–234.

Penman, H.L., 1948, Natural evaporation from open water, bare soil, and grass: Proceedings of the Royal Society of London, v. 193, no. 1032, p. 120–145.

PRISM Climate Group, 2017, Parameter-elevation Regressions on Independent Slopes Model (PRISM): Accessed August 1, 2017, at http://prism.oregonstate.edu.

R Core Team, 2017, R—A language and environment for statistical computing (x64 version 3.4.0): Vienna, Austria, R Foundation for Statistical Computing, accessed March 30, 2018, at https://www.R-project.org/.

Rice, S.E., and Crilley, D.M., 2014, Estimates of groundwater recharge rates and sources in the East Mountain area, Eastern Bernalillo County, New Mexico, 2005–12: U.S. Geological Survey Scientific Investigations Report 2014–5181, 24 p. [Also available at https://doi.org/10.3133/sir20145181.]

Rubel, F., Brugger, K., Haslinger, K., and Auer, I., 2017, The climate of the European Alps—Shift of very high resolution Köppen-Geiger climate zones 1800–2100: Meteorologische Zeitschrift, v. 26, no. 2, p. 115–125, accessed September 9, 2017, at http://koeppen-geiger.vu-wien.ac.at/.

Schaaf, C.B., Gao, F., Strahler, A.H., Lucht, W., Li, X., Tsang, T., Strugnell, N.C., Zhang, X., Jin, Y., Muller, J.-P., Lewis, P., Barnsley, M., Hobson, P., Disney, M., Roberts, G., Dunderdale, M., Doll, C., d'Entremont, R.P., Hu, B., Liang, S., Privette, J.L., and Roy, D., 2002, First operational BRDF, albedo nadir reflectance products from MODIS: Remote Sensing of Environment, v. 83, no. 1–2, p. 135–148.

Schneider, J.M., and Ford, D.L., 2011, Evaluating PRISM precipitation grid data as possible surrogates for station data at four sites in Oklahoma: Oklahoma Academy of Science Proceedings, v. 90, p. 93–104.

Senay, G.B., 2018, Technical Note—Satellite psychrometric formulation of the Operational Simplified Surface Energy Balance (SSEBop) model for quantifying and mapping evapotranspiration: Applied Engineering in Agriculture, v. 34, no. 3, p. 555–566. [Also available at https://doi.org/10.13031/aea.12614.]

Senay, G.B., Budde, M., Verdin, J.P., and Melesse, A.M., 2007, A coupled remote sensing and simplified surface energy balance approach to estimate actual evapotranspiration from irrigated fields: Sensors, v. 7, no. 6, p. 979–1000.

Senay, G.B., Bohms, S., Singh, R.K., Gowda, P.H., Velpuri, N.M., Alemu, H., and Verdin, J.P., 2013, Operational evapotranspiration mapping using remote sensing and weather datasets—A new parameterization for the SSEB approach: Journal of the American Water Resources Association (JAWRA), v. 49, no. 3, p. 577–591. [Also available at https://doi.org/10.1111/jawr.12057.]

Senay, G.B., Friedrichs, M., Singh, R.K., and Velpuri, N.M., 2016, Evaluating Landsat 8 evapotranspiration for water use mapping in the Colorado River Basin: Remote Sensing of Environment, v. 185, p. 171–185. [Also available at https://doi.org/10.1016/j.rse.2015.12.043.]

Senay, G.B., Schauer, M., Friedrichs, M., Velpuri, N.M., and Singh, R.K., 2017, Satellite-based water use dynamics using historical Landsat data (1984–2014) in the southwestern United States: Remote Sensing of Environment, v. 202, p. 98–112. [Also available at https://doi.org/10.1016/j.rse.2017.05.005.]

Senay, G.B., Schauer, M., Velpuri, N.M., Singh, R.K., Kagone, S., Friedrichs, M., Litvak, M., and Douglas-Mankin, K.R., 2019, Long-term (1986–2015) crop water use characterization over the Upper Rio Grande Basin using Landsat-based evapotranspiration: Remote Sensing, v. 11, no. 13, article 1587, 25 p. [Also available at https://doi.org/10.3390/rs11131587.]

Shuttleworth, W.J., 1993, Evaporation, chap. 4 *of* Maidment, D., ed., Handbook of hydrology: New York, McGraw-Hill, p. 4.1–4.53.

Sobrino, J.A., Jiménez-Muñoz, J.C., and Paolini, L., 2004, Land surface temperature retrieval from LANDSAT TM 5: Remote Sensing of Environment, v. 90, p. 434–440. [Also available at https://doi.org/10.1016/j.rse.2004.02.003.]

Soil Survey Staff, Natural Resources Conservation Service [NRCS], 2012, Soil Survey Geographic (SSURGO) Database: U.S. Department of Agriculture website, accessed July 11, 2017, at http://sdmdataaccess.nrcs.usda.gov/.

Soil Survey Staff, Natural Resources Conservation Service [NRCS], 2017, Web soil survey: U.S. Department of Agriculture website, accessed June 25, 2017, at https://websoilsurvey.sc.egov.usda.gov/.

Su, Z., 2002, The surface energy balance system (SEBS) for estimation of turbulent fluxes: Hydrology and Earth Systems Sciences, v. 6, no. 1, p. 85–100.

Thornton, P.E., Thornton, M.M., Mayer, B.W., Wilhelmi, N., Wei, Y., Devarakonda, R., and Cook, R.B., 2014, Daymet—Daily surface weather data on a 1-km grid for North America, version 2. Data set: Oak Ridge, Tenn., Oak Ridge National Laboratory Distributed Active Archive Center. [Also available at https://doi.org/10.3334/ORNLDAAC/1219.]

U.S. Census Bureau, 2010, Community facts: U.S. Census Bureau website accessed September 9, 2017, at http://factfinder.census.gov.

Verger, A., Baret, F., Weiss, M., Filella, I., and Penuelas, J., 2015, GEOCLIM—A global climatology of LAI, FAPAR, and FCOVER from VEGETATION observations for 1999–2010: Remote Sensing of Environment, v. 166, p. 126–137. [Also available at https://doi.org/10.1016/j.rse.2015.05.027.]

Wang T., Hamann A., Spittlehouse D., and Aitken S., 2006, Development of scale-free climate data for Western Canada for use in resource management: International Journal of Climatology, v. 26, no. 3, p. 383–397.

Ward, A.D., Trimble, S.W., and Wolman, M.G., 2004, Evaporation, chap. 4 *of* Environmental Hydrology (2d ed.): Boca Raton, Fla., CRC Press, p. 83–117.

Wildland Fire Science, Earth Resources Observation and Science [EROS] Center, 2016, LANDFIRE existing vegetation types and cover datasets: U.S. Geological Survey website, accessed September 13, 2017, at https://www.landfire.gov/vegetation.php.

For more information about this publication, contact
Director, New Mexico Water Science Center
U.S. Geological Survey
6700 Edith Blvd. NE
Albuquerque, NM 87113

For additional information visit
https://www.usgs.gov/centers/nm-water

Publishing support provided by
Lafayette Publishing Service Center

ISSN 2328-0328 (online)
https://doi.org/10.3133/sir20205095